Copyright Warning & Restrictions

The copyright law of the United States (Title 17, United States Code) governs the making of photocopies or other reproductions of copyrighted material.

Under certain conditions specified in the law, libraries and archives are authorized to furnish a photocopy or other reproduction. One of these specified conditions is that the photocopy or reproduction is not to be "used for any purpose other than private study, scholarship, or research." If a, user makes a request for, or later uses, a photocopy or reproduction for purposes in excess of "fair use" that user may be liable for copyright infringement,

This institution reserves the right to refuse to accept a copying order if, in its judgment, fulfillment of the order would involve violation of copyright law.

Please Note: The author retains the copyright while the New Jersey Institute of Technology reserves the right to distribute this thesis or dissertation

Printing note: If you do not wish to print this page, then select "Pages from: first page # to: last page #" on the print dialog screen

NJIT
New Jersey's Science &
Technology University

The Van Houten library has removed some of the personal information and all signatures from the approval page and biographical sketches of theses and dissertations in order to protect the identity of NJIT graduates and faculty.

ABSTRACT

THERMOELECTRIC PROPERTIES OF SILICON-GERMANIUM ALLOYS

by

Maske Aniket Annasaheb

Direct energy conversion from thermal to electrical energy, based on thermoelectric effects, is attractive for potential applications in waste heat recovery and environmentally friendly refrigeration. The energy conversion efficiency of thermoelectric devices is related to the thermoelectric figure of merit ZT, which is proportional to the electrical conductivity, the square of the Seebeck coefficient, and the inverse of the thermal conductivity. Currently, the low ZT values of available materials restrict the large scale applications of this technology. Recently, however, significant enhancements in ZT have been reported in nanostructured materials such as super-lattices mainly due to their low thermal conductivities. According to the studies on heat transfer mechanisms in nanostructures, the reduced thermal conductivity of nanostructures is mainly attributed to the increased scattering of phonons at the interfaces. Based on this idea, nanocomposites are also expected to have a lower thermal conductivity than their bulk counterparts of the same chemical configuration. Nanocomposites are materials with constituents of less than 100 nm in size. They can be fabricated at low cost by mixing nano-sized particles followed by consolidation of nano-sized powders.

In this thesis, SiGe nanocomposites are investigated for various parameters, such as thermal conductivity, electrical conductivity and Seebeck coefficient, which are needed for thermoelectrics. Grain boundaries in nanocomposites can scatter phonons,

when their mean free path is longer than the grain size. Mean free path of electrons is usually shorter than the grain size of nanocomposites, so that the electrical conductivities of nanocomposites are not expected to change significantly. However, the results show that, at the nano scale, the electron transport properties are affected. The electronic and thermal properties are calculated using MATLAB software. The results are compared with the literature. The studies show an enhancement in ZT for n-type and p-type SiGe alloys mostly due to the reduction in the thermal conductivity. Such a reduction is due to both the alloying effect and increased phonon interface scattering at grain boundaries.

THERMOELECTRIC PROPERTIES OF SILICON-GERMANIUM ALLOYS

By

Maske Aniket Annasaheb

A Thesis
Submitted to the Faculty of
New Jersey Institute of Technology
in Partial Fulfillment of the Requirements for the Degree of
Master of Science in Materials Science and Engineering

Interdisciplinary Program in Materials Science and Engineering

January 2016

APPROVAL PAGE

THERMOELECTRIC PROPERTIES OF SILICON-GERMANIUM ALLOYS

Aniket Annasaheb Maske

Dr. N. M. Ravindra, Thesis Advisor Date
Professor, Department of Physics
Director, Interdisciplinary Program in Materials Science & Engineering, NJIT

Dr. Michael Jaffe, Committee Member Date
Research Professor, Department of Biomedical Engineering, NJIT

Dr. Eon Soo Lee, Committee Member Date
Assistant Professor, Department of Mechanical & Industrial Engineering, NJIT

BIOGRAPHICAL SKETCH

Author: Maske Aniket Annasaheb

Degree: Master of Science

Date: January 2016

Undergraduate and Graduate Education:

- Master of Science in Materials Science and Engineering,
  New Jersey Institute of Technology, Newark, NJ, 2016
- Bachelor of Technology in Metallurgical & Materials Engineering,
  College of Engineering, Pune, Maharashtra, India, 2013

Major: Materials Science and Engineering

ACKNOWLEDGEMENTS

The end of my graduate studies is a good time to stop and give thanks to all those who helped me to get to this milestone. As I complete my Master's degree, the end of over twenty years of schooling leaves me with some trepidation, but also excitement at the possibilities that await me. Without those who have guided me along the way, the arc of my life, and correspondingly this dissertation, would have been far different.

First and foremost, I would like to thank Prof. N. M. Ravindra, my advisor. To my knowledge, a professor is a mentor, a teacher, and a scholar all in one. Prof. Ravindra exemplifies the best in each of these roles. I really appreciate his help when I most needed it, he stood by me. I cannot adequately express in words my sincere thanks to my thesis committee members, Dr. Michael Jaffe and Dr. Eon Soo Lee. I thank my thesis committee members for their helpful comments and discussions. I felt deeply privileged to work with them.

I am thankful to the developers of the Open-Source software codes for MATLAB, which made it easier to work with the complicated equations that describe the properties of thermoelectrics.

I acknowledge with thanks the input from Ms. Clarisa Gonzalez-Lenahan, Associate Director of Graduate Studies, Mrs. Lillian Quiles, Administrative Assistant of Graduate Studies, NJIT, for formatting and improving the presentation of my thesis.

I would like to thank my parents and friends for all they have done for me. Their unending expression of love and pride in my choices allowed me to take risks in my educational path.

I would like to dedicate this work to

my parents, Dr. Annasaheb H. Maske and Mrs. Kalpana A. Maske,

my family, Ketki A. Maske, Dr. Sonal Mandale, Dr. Vilas S. Kharat ,

and friends, Mr. Sagar M. Ghateshai, Mr. Vishal Nakathe

for their continuous support and motivation in my life !

TABLE OF CONTENTS

Chapter		Page
1	INTRODUCTION …….	1
2	THERMOELECTRICS …….	2
	2.1 Phenomenological Approach to Thermoelectrics ……..	5
	2.1.1 The Seebeck Effect ……..	5
	2.1.2 Peltier and Thomson Effects ……	6
	2.1.3 Basic Principles and Thermoelectric Coefficients …….	8
	2.1.4 Optimizing the Thermoelectric Properties of Materials …….	11
	2.1.5 Thermoelectric Device Efficiency ……...	13
	2.1.6 Nanostructure for Thermoelectric Efficiency ……..	16
	2.2 Basic Concepts in Electron and Heat Transport …….	17
	2.2.1 Electron Transport in Bulk Materials ……..	17
	2.2.2 Phonon Transport in Bulk Materials ……	28
3	FIGURE OF MERIT …….	38
	3.1 Strategies to Enhance ZT with Novel Approaches …….	40
	3.2 Nanostructured Thermoelectric Materials ……..	40
	3.3 Future Research in Nanocomposites ……..	42
4	SiGe- AS THERMOELECTRIC MATERIALS ……...	44
	4.1 Material Introduction ……..	44
	4.2 History of SiGe Alloys as Thermoelectrics ……	45
	4.3 Properties of p-, n- Type $Si_{80}Ge_{20}$ Alloys ……..	47

TABLE OF CONTENTS
(Continued)

Chapter		Page
	4.4 Recent Advances in SiGe Alloys ……	52
5	PROPERTY MODELING …….	54
	5.1 Bulk Modeling …….....	55
	5.2 Charge Transport in Nanocomposites ……	61
	5.3 MATLAB ……...	66
6	RESULTS AND DISCUSSION ……	67
	6.1 n-Type SiGe ……...	68
	6.2 p-Type SiGe ……...	72
7	CONCLUSIONS ……...	75
8	REFERENCES ……..	77

LIST OF FIGURES

Figure		Page
2.1	(a) Thermoelectric Power Generator (b) Heating and Cooling applications of Thermoelectric devices……	4
2.2	The experimental device used by Seebeck to discover the first Thermoelectric Effect ……..	6
2.3	Peltier Effect flow diagram …….	7
2.4	A Basic Thermoelectric circuit ……..	9
2.5	(a) A schematic diagram of thermoelectric cooler. (b) Instead of passing current through the device, a temperature gradient can be created by applying two different temperatures on the two sides to produce a voltage difference ……	14
2.6	(a) p-type materials (b) n-type materials …….	16
2.7	ZnS Sphalerite, *B*3 Type Structure ……..	19
2.8	ZnS Crystal Structure showing both Zincblende and Wurtzite Structures……..	20
2.9	Rock Salt Structure (NaCl) ……..	21
2.10	Energy band diagram of (a) Germanium, (b) Silicon and (c) Gallium Arsenide……...	22
2.11	Electron scattering Mechanisms …….	26
2.12	One dimensional representation of atoms and chemical bond as spring mass system…….…….	29
2.13	Dispersion Relation of Phonons ……..	30
2.14	(a) Vectorial representation of a normal phonon scattering where two phonons combine to create a third. (b) Normal processes where one phonon scatters into two phonons. (c) Umklapp processes where two phonons combine to create third……...	33

LIST OF FIGURES
(Continued)

Figure		Page
3.1	Evolution of the Maximum ZT over Time ……..	39
4.1	Electrical conductivity and Seebeck coefficient plotted versus carrier concentration ……	44
4.2	Modern day ZT values …….	45
4.3	Sample of Si/Ge crystal structure ……	48
4.4	The specific heat of typical thermoelectric SiGe …….	49
4.5	The resistivity of typical thermoelectric SiGe …….	50
4.6	The thermo-power of typical thermoelectric SiGe ……..	50
4.7	The total thermal conductivity of typical thermoelectric SiGe ……...	51
4.8	The ZT of typical thermoelectric SiGe ……	52
5.1	Relaxation time for different scattering mechanisms for (a) different electron energies, (b) for various temperature range …….....	58
5.2	Optimization of ZT with respect to carrier concentration, considering electron grain boundary scattering. (a) Electrical Conductivity, (b) Seebeck Coefficient, (c) Power Factor, (d) ZT……	63
5.3	Optimization of ZT with respect to grain size. (a) Power Factor, (b) Lattice Thermal Conductivity, (c) ZT……..	65
6.1	Thermal Conductivity versus Temperature Graph (n-type $Si_{80}Ge_{20}$)…...	68
6.2	Electrical Conductivity versus Temperature Graph (n-type $Si_{80}Ge_{20}$)…	69
6.3	Seebeck Coeeficient versus Temperature Graph (n-type $Si_{80}Ge_{20}$)…….	69
6.4	ZT VS Temperature Graph (n-type $Si_{80}Ge_{20}$)……..	70
6.5	Electrical Conductivity versus Temperature Graph (p-type $Si_{80}Ge_{20}$)…	72
6.6	Seebeck Coefficient versus Temperature Graph (p-type $Si_{80}Ge_{20}$)…….	73
6.7	Power Factor versus Temperature Graph (p-type $Si_{80}Ge_{20}$)…….	73

LIST OF FIGURES
(Continued)

Figure **Page**

6.8 Thermal Conductivity versus Temperature Graph (p-type $Si_{80}Ge_{20}$)… 74

6.9 ZT versus Temperature Graph (p-type $Si_{80}Ge_{20}$)…… 74

LIST OF TABLES

Table		Page
3.1	Material Properties of SiGe and Si …….	42
5.1	Electron Modeling Parameters ……...	57
5.2	Phonon Modeling Parameters ……	60

CHAPTER 1

INTRODUCTION

In this thesis, the thermoelectric properties of Silicon-Germanium (SiGe) alloys are studied. The details of this study are presented in seven chapters.

The second chapter of this thesis focuses on the fundamentals of thermoelectric properties. This chapter also focuses on the electron and phonon effects on thermoelectric properties. A literature survey of the thermoelectric properties of various materials is presented in this chapter. The basics of heat conduction, phonon dispersion and electronic properties of SiGe alloys are presented. Thermoelectric Properties of SiGe alloys of both bulk and nano-scale are discussed.

The third chapter focuses on the factors affecting the Figure of Merit in SiGe alloys. Approaches to increase the Figure of Merit, by various methods, are discussed.

The fourth chapter begins with the basics of Silicon-Germanium alloys. The fundamental properties of SiGe alloys at the bulk and nano-scale are explained in this chapter.

The fifth chapter deals with the computational methods that are utilized to simulate the various parameters that are needed to calculate the Figure of Merit. Computational methods, based on MATLAB, are used for calculating the various properties of SiGe alloys.

The sixth chapter focuses on results and discussion. The various results, obtained in this study, are discussed and compared with the literature.

The seventh chapter is the conclusion and recommendations followed by reference

CHAPTER 2

THERMOELECTRICS

The ever-increasing amounts of electricity needed in everyday life and the well-known scarcity of fossil–fuel reserves, have catalyzed the search and research for alternative energy sources as one of the major challenges of the 21st century. Much effort is being invested in this direction, to lower the damage caused by carbon-based combustion to the environment. However, considering the enormity of the problem, every effort is welcome, so that not only research on potential resources to substitute fossil fuels, such as photovoltaics, wind power technology or hydrogen-based technologies must be encouraged, but also research devoted to improve the current fuel efficiencies must be followed. Nowadays, most of the energy produced is lost in terms of heat, mainly in electrical power generation and transport. For instance, from the electrical energy for consumption in houses, around 60% of the energy extracted from power plants is lost as waste heat during its generation [1], and between 8% and 15% is lost as heat in the electrical lines for its transport and transformation [2]. Therefore, only around 35% of the total energy produced in a power plant reaches houses. Another example is the efficiency in transportation, where 40% of the energy produced in a car is wasted as heat and another 30% of the total is used for cooling the engine, making a total of 70% of wasted energy, and this is without taking into account the CO_2 emissions to the atmosphere produced by this extra 70% of fuel that has to be used. It is in this situation where thermoelectric materials can contribute to be part of the solution to have a more

sustainable world, taking advantage of their ability to convert temperature differences into electrical power, which is, obtaining power from wasted heat [1, 2].

As of today, most energy resources are consumed as thermal energy, with an average yield around 30 %. The remaining 70 % are wasted and the major part of this residual energy is rejected in the environment in the form of thermal energy. This thermal energy is wasted and is difficult to recycle using traditional conversion methods since it is typically associated with temperature ranges below 700 K. It presents strong variations in power density and is stored in various environments [1-3].

This is why, over the past ten years, there has been a growing interest in thermoelectric materials, which have the unique property to convert heat into electricity, and vice-versa. Such a conversion is very interesting since electricity can be stored and used for many different applications. Moreover, thermoelectric conversion presents numerous advantages, such as no need for maintenance, the lack of dependence on the type of heat source, the easy setup or even the longevity of this technology (related to the absence of moving parts). Thermoelectric generators are composed of different modules which contains p-type and n-type semiconducting materials. The diffused heat goes hand in hand with the diffusion of charge carriers, in the same direction, which produces a voltage.

Due to their associated weak efficiency, thermoelectric generators are not yet widely exploited. However, there is significant anticipation to use them, in combination with other devices, in power plants for recovering waste heat and converting it into additional sources of electrical power [4]. They have also been used in space probes, using radioisotopes as heat sources. Some devices are also set up inside the exhaust pipe

of automobiles to convert waste heat into electricity. These devices are called "Automotive Thermoelectric Generators" [3].

Thermoelectrics can also be used for cooling applications. These thermoelectric coolers are most widely used and are mostly known as "Peltier coolers" [3]. They are mainly used to cool electronic components, but are also used for many consumer products, such as camping/car coolers. They have proven themselves to be precise temperature regulators (error around 0.01 K) with the necessary electronic feedback.

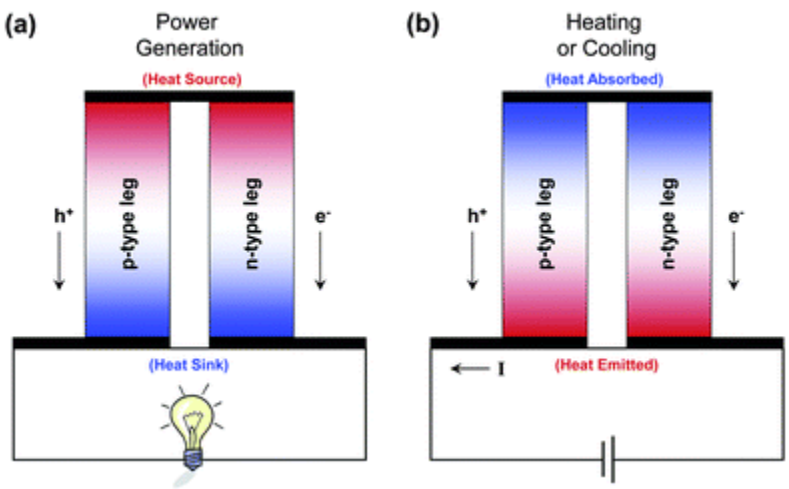

Figure 2.1 (a) Thermoelectric Power Generator (b) Heating and Cooling application of Thermoelectric devices.

Source: Jeannine R. Szczech, Jeremy M. Higgins and Song Jin, Enhancement of the thermoelectric properties in nanoscale and nanostructured materials, *J. Mater. Chem.*, 2011, 21, 4037-4055 doi: 10.1039/c0jm02755c

One can expect that enhancing thermoelectric performance would lead to a greater amount of mainstream applications that could be coupled with other energy converters such as photovoltaics, which fail to utilize the thermal part of solar energy. Even without challenging other traditional means for converting heat into electricity, using thermoelectrics to convert waste energy into usable energy is a sufficient

motivation to use them; irrespective of the amount, energy is to be gained in the process. These are examples among many others, but basically, thermoelectrics could play an important role in the future [5].

2.1 Phenomenological Approach to Thermoelectrics

This section presents a historical introduction to thermoelectricity, from the discovery of the phenomenon to the characterization of the performance of thermoelectrics.

2.1.1 The Seebeck Effect

Thomas Johann Seebeck discovered the first thermoelectric effect in 1821 [6]. He observed that when a metallic compass needle is placed in between two different conductors ‘a’ and ‘b’, linked by junctions at their extremities and under a temperature gradient, the needle is detected (as shown in Figure 2.1). This was because the metals responded to the temperature difference in different ways, creating a current loop and a magnetic field. Seebeck did not recognize that there was an electric current involved; so he called the phenomenon the thermomagnetic effect. Danish physicist Hans Christian Ørsted rectified this and coined the term "Thermoelectricity". Thus, thermoelectricity was discovered [5, 6].

Historically, the main use of the Seebeck effect is to measure temperature with a thermocouple. In general, the Seebeck effect is described locally by the creation of an electromotive field.

The Seebeck coefficient (S), or thermoelectric power (thermopower), of a material is the measure of the magnitude of an induced voltage in response to the temperature gradient across that material. It can be written as:

$$E = S_{ab} \nabla_r T \tag{2.1}$$

where, E is the electric field induced by the temperature gradient $\nabla_r T$.

The Seebeck coefficients (S_{ab}) generally vary as function of temperature, and depend strongly on the composition of the conductor [4].

Figure 2.2 The experimental device used by Seebeck to discover the first thermoelectric effect.

Source: Lemal Sebastien, Ph. Ghosez , First-principles study of the electronic and thermoelectric properties of $Ca_3Co_4O_9$, (2013), pp 12.

2.1.2 Peltier and Thomson Effects

In 1834, Jean Charles Athanase Peltier discovered a second thermoelectric effect: a temperature gradient would appear at the junctions of two different materials ‘a’ and ‘b’ in which a voltage is applied. In other words, when a current is flowing through the junction, one junction absorbs heat while the other generates it [3].

Thus, another coefficient is defined: the Peltier coefficient measures the magnitude of produced and absorbed heat at the junction when a current is applied:

$$Q = \prod_{ab} I \qquad (2.2)$$

with Q being the produced or absorbed heat, I being the electric current and $\prod_{ab}$ being the Peltier coefficient for the couple 'a' and 'b' .

In 1851, Lord Kelvin, predicted and observed that both Seebeck and Peltier effects are related: a single material under a temperature gradient and which is traversed by an electric current exchanges heat with the environment [6]. Reciprocally, an electric current is generated when a material is under a temperature gradient with heat flowing through. This phenomenon is called the "Thomson Effect". The main difference between the Peltier and Seebeck effects is that the Thomson effect involves only one material and no junction is required.

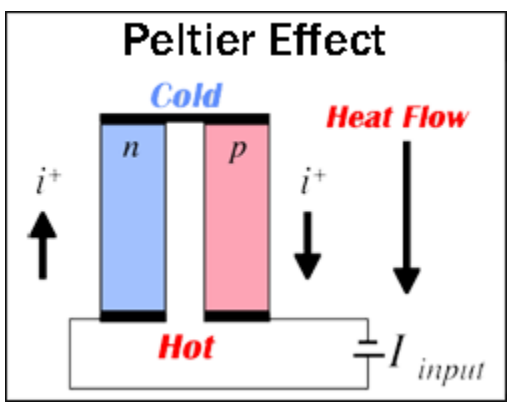

Figure 2.3 Peltier Effect flow diagram.

Source: Lemal Sebastien, Ph. Ghosez, First-principles study of the electronic and thermoelectric properties of $Ca_3Co_4O_9$, (2013), pp 1.

Thomson effect offers many perspectives. In one way, thermoelectic materials could be used as refrigerators; they can be used in many applications which require a highly precise temperature regulation. Alternatively, converting heat into electricity would represent a clean energy source, which is particularly interesting as mankind aspires to respect Earth and its environment better than it used to. [5]

2.1.3 Basic Principles and Thermoelectric Coefficients

We will now introduce the different relations involved in thermoelectricity. Let us consider a basic thermoelectric circuit. Two materials ‘a’ and ‘b’ linked together by two junctions, which we call ‘X’ and ‘W’. In the case of Seebeck effect, a difference of temperature dT is applied between the two junctions X and W, which generates a voltage dV between the extremities ‘Y’ and ‘Z’ (Figure 2.4) [6]. In an open circuit, the Seebeck coefficient is defined for the couple ‘a’ and ‘b’:

$$S_{ab} = dV/dT \tag{2.3}$$

The sign of $\mathbf{S_{ab}}$ is such as if the temperature at the junction “W” is higher than the temperature at the junction X, and if VY > VZ, then $\mathbf{S_{ab}}$ is positive.

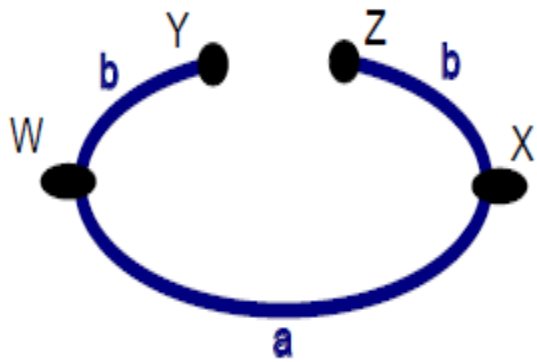

Figure 2.4 A Basic Thermoelectric circuit.

Source: Lemal Sebastien, Ph. Ghosez , First-principles study of the electronic and thermoelectric properties of $Ca_3Co_4O_9$, (2013).

In the case of the Peltier effect, a current *I* is flowing through the circuit. Heat is then absorbed at one junction, and produced at the other. The Peltier coefficient is defined for the couple 'a' and 'b':

$$\prod ab = \frac{Q}{I} \tag{2.4}$$

The sign of $\prod_{ab}$ is such as if the current goes from W to X and if the absorption of heat occurs at the junction W, and the production of heat occurs at the junction X, then $\prod_{ab}$ is positive [7].

In the case of the Thomson effect, both an electric current and a temperature gradient are applied. Heat is then generated or absorbed in each part 'a' and 'b' of the thermocouple individually. The thermal flux in each material is given by the relation:

$$\frac{dQ}{dz} = \tau\, I\, \frac{dT}{dz} \tag{2.5}$$

where, z is the spatial coordinate and $\boldsymbol{\tau}$ is the Thomson coefficient of the material. These three effects are related, and it was demonstrated by Kelvin that each coefficient characterizing these three effects are also related. The relations are:

$$\prod_{ab} = S_{ab} \tag{2.6}$$

In practice, applications for thermoelectric effects require at least two materials linked together to form junctions.

$$\tau_a - \tau_b = T \frac{dSab}{dT} \tag{2.7}$$

The Seebeck coefficient and Peltier coefficients have been defined for the couple of materials - ‘a’ and ‘b’. The absolute coefficients are given by:

$$S_{ab} = S_a - S \tag{2.8}$$

However, the knowledge of the absolute coefficients of each material (S_a, S_b, $\prod_a$ and $\prod_b$) is important for their own optimization.

$$\prod_{ab} = \prod_a - \prod_b \tag{2.9}$$

When one measures the thermopower of a couple of materials, one usually measures the contribution from both part of the thermocouple. But it is possible to measure the absolute Seebeck coefficient of a material by using superconductors. Indeed, in a superconductor, electrons do not carry entropy, and thus superconductors have zero thermopower. The absolute Seebeck, Peltier and Thomson coefficients also obey the relations of Lord Kelvin [7]:

$$\prod_a = S_a T \tag{2.10}$$

and

$$\tau_a = T \frac{dSa}{dT} \tag{2.11}$$

2.1.4 Optimizing the Thermoelectric Properties of Materials

Improving the thermoelectric performance of a material can be achieved by increasing its "Factor of Merit" or equivalently it is dimensionless "Figure of Merit":

$$ZT = \frac{T\sigma}{k} S^2 \tag{2.12}$$

where ZT is figure of merit, S is the seebeck coefficient, T is the temperature, k is total thermal conductivity and σ is electrical conductivity. The numerator $S^2 \sigma$ is also called "Power Factor" that one should maximize. The denominator, total thermal conductivity k, should be minimized [8] in order to maximize ***ZT***. More detailed discussion to increase the figure of merit and factors affecting it will be discussed in the coming chapters.

Often, both the electrical and thermal conductivities are related. For metals, the ratio between electronic thermal conductivity, k and electrical conductivity σ , follows the Wiedemann-Franz law:

$$\frac{k}{\sigma} = LT \tag{2.13}$$

with L is being a constant and T being the temperature. In other words, at a fixed temperature, the ratio $\frac{k}{\sigma}$ stay the same and if one increases σ, k should also increase. This behavior can be extrapolated to other materials and basically, optimizing these coefficients in opposition ends up being quite tricky. To get an optimum device performance, this figure of merit should be maximized. Materials with highest Seebeck coefficient, in general, have low thermal conductivity but are also poor conductors of electricity. On the other hand, metals have high electrical conductivity but thermal conductivity is also very high and Seebeck coefficient is small. The properties of semiconductors which lie between metals and insulators are best for thermoelectric properties [7, 8].

The recent progress in increasing the figure of merit finds its origin in many concepts and ideas which have been proposed in order to get rid of the interdependence of electrical and thermal conductivities. For example, an interesting and intriguing idea to achieve the highest figure of merit was proposed by Slack [9] and is referred to as the "Phonon - Glass Electron - Crystal Approach" (PGEC). Basically, a PGEC material features a very low thermal conductivity that is normally associated with amorphous materials, but a high electrical conductivity normally associated with good semiconductor single crystals.

Another idea proposed by Hick and Dresselhaus [10] is to confine the electrons in planes forming so-called "Two-Dimensional Electron Gas" (2DEG) in order to yield enhancement of the electrical conductivity. This can typically be realized in nanostructures that further enhance thermal resistivity by increasing phonon scattering at the interfaces between different layers.

In spite of intense studies, Bi_2Te_3, with a figure of merit as high as 1, still remains among the most powerful thermoelectrics since its discovery six decades ago (with a power factor around 40-50 $\mu Wcm^{-1}K^{-2}$ at room temperature) [11]. Nevertheless, the recent concepts and advancements in the field led to the discovery of other materials that exceed the performance of Bi_2Te_3 compounds, such as Bi_2Te_3/Sb_2Te_3 super-lattices which reach ZT = 2.4 [12]. Yet, in order for thermoelectricity to be used in large scale applications and to become competitive against alternative energy sources, the figure of merit should be at least 3 or more [10-12].

However, for some practical applications, research focuses on improving the power factor only instead of the figure of merit. This is typically the case for recovering wasted heat. A large power factor implies large voltage generation during the conversion process. In this case, the power factor is considered as the key quantity to optimize in order to achieve high thermoelectric efficiency. The present study focuses on this aspect of thermoelectrics.

2.1.5 Thermoelectric Device Efficiency

A schematic diagram of thermoelectric cooler is shown in Figure 2.5 (a). From this figure, several desired material properties become clear. This cooler (also known as "Peltier cooler") is made of two legs, one of which is n-type and contains mobile electrons and the other leg is p-type which has positive charges (holes). These two legs are connected electrically in series and thermally in parallel. When the current is passed through the legs along the direction shown, both the electrons and holes flow from the top

of the device towards the bottom and carry heat from the junction at the top of the device towards the base, cooling the junction at the top [12, 13].

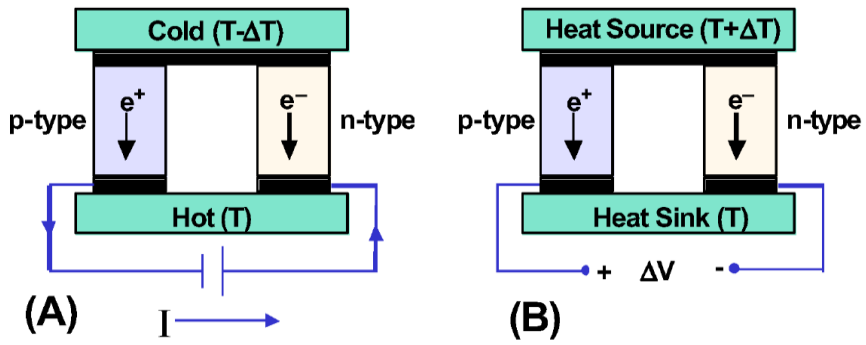

Figure 2.5 (a) A schematic diagram of thermoelectric cooler. Two electrically conducting legs are connected by a metal (black bar) at the top to make a junction. The right leg is "n-type" and contains mobile electrons and the left leg is "p-type" which has positive charges (holes). When the current flows in the direction shown, both electrons and holes flow away from the top of the device towards the bottom. In this process, they carry energy in the form of heat from the cold side to hot side. (b) Instead of passing current through the device, a temperature gradient can be created by applying two different temperatures on the two sides to produce a voltage difference as shown.

Source: Chandan Bera. Thermoelectric properties of nanocomposite materials. Engineering Sciences. Ecole Centrale Paris, 2010. English. <NNT: 2010ECAP0027>.pg-5

Thermoelectric generator is the opposite of a Peltier cooler. Thermoelectric generator, as demonstrated in Figure 2.5 (b), generates power in the presence of an externally generated temperature gradient. In this case, both carriers conduct heat from the heated junction at the top to the cooled side at the base, and a voltage drop is generated between the electrodes at the bottom [12].

In addition to cooling the top junction, when current is passed, it results in Joule heating in each leg. The amount of Joule heating is equal to the square of current times

the electrical resistance of the materials. Therefore, materials with low resistivity are required. Additionally, to prevent the setback of flow of heat from hot to cold junction, upon reaching thermal equilibrium, low thermal conductivity is necessary. The important parameter is the Seebeck coefficient, which measures the voltage generated across the material due to a temperature difference [12]. From the above example of the thermoelectric power generator (TEG), it is clear that large Seebeck coefficient is desired to maximize the voltage output for a given temperature drop. The voltage (V) generated by a TEG is directly proportional to the number of couples (N) and the temperature difference (T) between the top and bottom sides of the TEG and the Seebeck coefficients of the n-type and p-type materials (S_n and S_p respectively).

$$V = N\,(S_p - S_n)\ \Delta T \tag{2.14}$$

Power output from a TEG is defined as,

$$\eta = \frac{Th - Tc}{Th}\,\frac{\sqrt{(1+ZT)} - 1}{\sqrt{(1+ZT)} + Tc/Th} \tag{2.15}$$

where, Th and Tc are the hot junction and cold junction temperature, T is the average temperature of the system between Th and Tc and ***ZT*** is the dimensionless figure of merit of the TE materials. ***ZT*** is defined in equation (2.12).

2.1.6 Nanostructure for Thermoelectric Efficiency

In the early stages of semiconductor physics, the applications focused on thermoelectrics (TE) rather than the applications in microelectronics. Several semiconductors were investigated for their potential applications in TE. At the end of 1950's, the best thermoelectric materials were found to be alloys of bismuth telluride and antimony, with ***ZT*** close to unity. Afterwards, few improvements in ***ZT*** were achieved during the next forty years. In the early 1990's, by using nanotechnology, strong improvements in ***ZT*** were reported and the new discovery showed that nanostructure materials have better ***ZT*** compared to bulk materials [14].

In the following plot, we can observe the recent improvements of thermoelectric figure of merit, ***ZT***, for both p-type and n-type materials which was below unity during half a century.

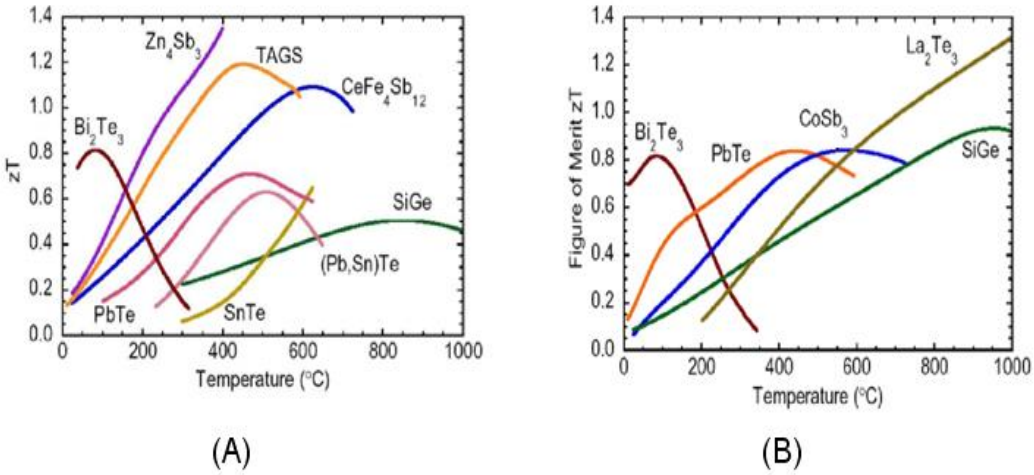

Figure 2.6 (a) p-type materials (b) n-type materials.

Source: Chandan Bera. Thermoelectric properties of nanocomposite materials. Engineering Sciences. Ecole Centrale Paris, 2010. English. <NNT : 2010ECAP0027>.

In 1990's, Hicks, Dresselhaus and Harman suggested [10,14,15] that the figure of merit could be improved if electrons were to be confined in two dimensions using the so called "Quantum Well Superlattices", where superlattices are multilayers of thin films on the order of several nanometers in thickness. Hicks and Dresselhaus later extended their work to include one-dimensional conductors such as nano-wires [12,15]. The primary reason for the enhancement in the figure of merit in these low-dimensional structures is through an increase in the electronic density of states per unit volume, which leads to an improved thermo-power. However, low-dimensional structures often exhibit a reduced thermal conductivity when compared to bulk materials [4,16]. In fact, in some instances, the benefits came from the suppressed thermal conductivity which may outweigh any gains due to electron confinement.

In order to study the thermoelectric properties, we need a detailed knowledge of the transport properties, such as mobility, diffusivity, carrier lifetime, and surface effect, which will now be presented.

2.2 Basic Concepts in Electron and Heat Transport

2.2.1 Electron Transport in Bulk Materials

The transport properties of electrons in a material are related to the energy band structure and the nature of collision processes. Again, the characteristics of the energy band structure are related to the crystal structure [12].

2.2.1.1 Crystal Structure Crystal structure is composed of a pattern, a set of atoms arranged in a particular way, and a lattice exhibiting long-range order and symmetry. Patterns are located on the points of a lattice, which is an array of points repeating periodically in three dimensions. The points can be thought of as forming identical tiny boxes, called “Unit Cells”, that fill the space of the lattice. The lengths of the edges of a unit cell and the angles between them are called the “lattice parameters”. The symmetry properties of the crystal are embodied in its space group. Most of the useful and well-known compound semiconductors have one of the three structures: that of zincblende (also known as sphalerite), the wurtzite (also known as zincite) or rock salt (also called sodium chloride) [12].

In zincblende structure, an atom of one kind constituting binary compound is surrounded by four equidistant atoms of another kind, which occupy the vertex of a tetrahedron, the atom of the first kind being at its center. The orientation of the neighboring atoms is such that the atoms also occupy the sites of two interpenetrating face-centered-cubic (fcc) lattice. The arsenides, antimonides, and phosphides of aluminium, indium, and gallium among the III-V compounds and sulphides, selenides, and tellurides of cadmium, zinc, and mercury among the II-VI compounds have the zincblende crystal structure. Most well-known semiconductors - silicon and germanium have essentially the same kind of crystal structure, but the two atoms forming the basis being similar, this type of structure is also known as the diamond structure, and has inversion symmetry [17].

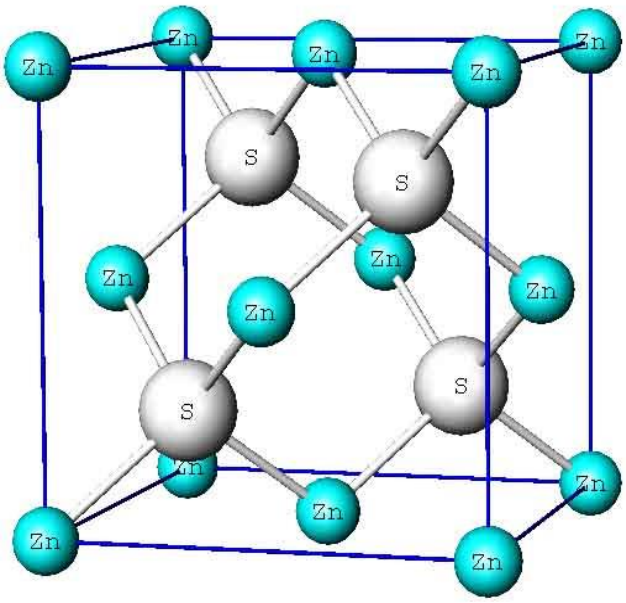

Figure 2.7 ZnS Sphalerite, *B*3 Type Structure.

Source: Sphalerite , http://www.geocities.jp/ohba_lab_ob_page/structure6.html (Accessed: 04/10/2015).

In the wurtzite structure, the basic arrangement of atoms is similar to the sphalerite structure. An atom of one kind is surrounded tetrahedrally by four atoms of another kind, but the tetrahedrons are oriented so that the location of the atoms fit two interpenetrating close-packed hexagonal lattices. In III-V compounds, the relatively unknown crystals of nitrides of aluminium, indium, and gallium have wurtzite structures. Most of the II-IV compounds have both a wurtzite and a sphalerite modification [18].

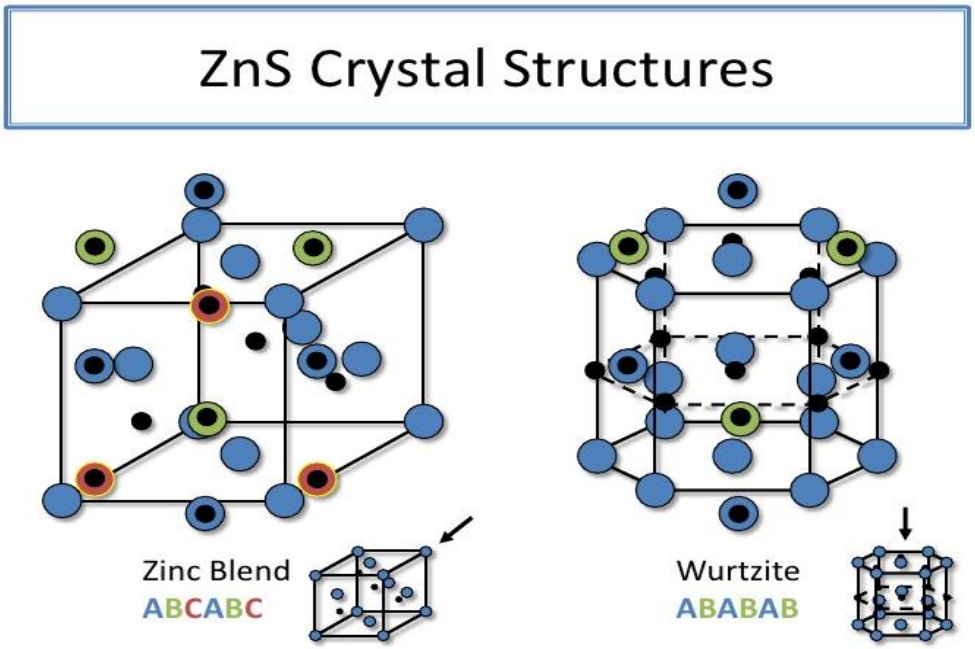

Figure 2.8 ZnS crystal structure showing both zincblende and wurtzite structures.

Source: Daniel Moore, Novel ZnS Nanostructures – Synthesis, Growth Mechanism and Application, Georgia Institute of Technology, Oct. 2006 (Accessed; 05/07/2015).

The arrangement of atoms in the rock-salt structure is such that atoms of the two kinds occupy alternate positions on a face-centered-cubic lattice. It may also be considered as two interpenetrating parallel face-centered lattices. The important compound semiconductors having the rock-salt structure are the sulphides, selenides, and tellurides of lead. The band structure of these materials have broad similarity with those of the sphalerite and wurtzite structure; however, due to the differences in the lengths of the basis vector, there are significant differences, the most important is the position of the valence band maxima and the shape of the associated constant energy surface [19,20].

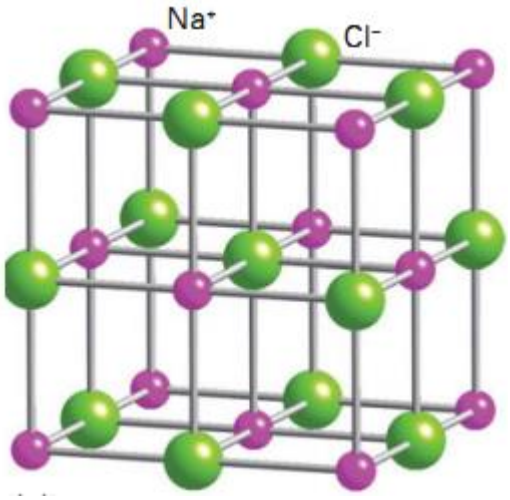

Figure 2.9 Rock Salt Structure (NaCl).

Source: Rock Salt Structure, http://chemistrytextbookcrawl.blogspot.com/2012/08/rock-salt-structure.html, (Accessed: 09/06/2015).

2.2.1.2 Energy Band The forms of the energy bands are determined by the crystal structure. Information related to the band structure is generally presented by plotting the energy of electron, E for the value of wave vector, k, limited to within the first Brillouin zone [21]. When we consider the transport properties of different materials, we are mainly concerned with the extrema of energy band. For different materials, the properties change depending on the position of these extremes of the band and on the effective mass, m*, of the band [4].

The characteristics of the energy bands are usually indicated by plotting the energy Eigen values of the electrons for different values of k in the Brillouin zone. The crystal potential is different in different directions because of the differences in the spacing of the atoms. Therefore, the values of E depend on both the magnitude and the directions of k. In the case of transport problem, we are generally concerned with the

lowest minima and the highest maxima as these are populated respectively by electrons and holes. From Figure 2.10, it is clearly understood that the conduction band is higher than the valence band, has minima at the zone center (Γ point) and one minima in the < 111 > direction and another in the < 100 > direction. The valence band, which is below the conduction band, is separated by an energy gap for the insulator or semiconductor, and generally has a maxima at the zone center.

If the energy E varies parabolically with ($\bar{k}$ –$\bar{k}_0$), where $\bar{k}_0$ is the values of $\bar{k}$ at the extremum, the relation between E and $\bar{k}$ at the Γ point can be expressed as [22]:

$$E=\frac{\hbar^2 k^2}{2m^*} \tag{2.16}$$

where, ħ is the reduced Planck's constant and m* is the effective mass of the charge carrier. For the Γ - point, m* is a scalar quantity.

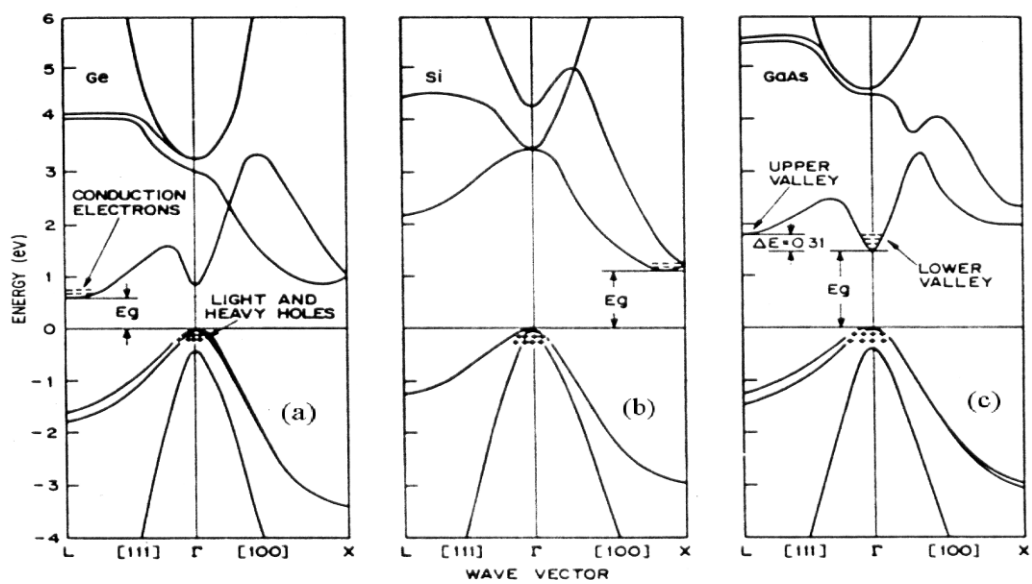

Figure 2.10 Energy band diagrams of (a) Germanium, (b) Silicon and (c) Gallium Arsenide.

Source: Energy bands. http://ecee.colorado.edu/~bart/ecen3320/newbook/chapter2/ch2 3.htm. (Accessed: 12/10/2015)

The E - $\bar{k}$ relation for the minima lying on the X and L directions is of the form

$$E=\frac{\hbar^2}{2}\left(\frac{k_l^2}{m_l}+\frac{k_t^2}{m_t}\right) \tag{2.17}$$

where, k_l and k_t represent respectively the components of $\bar{k}$ in a direction parallel to the direction of symmetry, measured from the position of the minimum, and in the transverse direction. The constant energy surfaces are spheroidal, and the shape of the spheroid is generally prolate. The effective mass for these minima are tensor quantity, the tensor being diagonal, with diagonal quantity m_l, m_t, and m_t, when a direction of symmetry corresponding to the particular minimum is chosen as a reference axis.[21,22]

In some cases, the energy E for points in $\bar{k}$ space, away from the extrema, varies nonparabolically with $\bar{k}$. In that case, the nonparabolic E - $\bar{k}$ relation can be written as: [36],

$$E(1+\alpha E) = \frac{\hbar^2 k^2}{2m^*} \tag{2.18}$$

where, m* is the effective mass for k tending to zero, and α is a constant which in many materials is approximately equal to $1=E_g$, E_g being the separation between the conduction band minimum and valence band maximum, i.e. band gap.

There are different methods to solve the energy band structure of materials. The detailed nature of the energy band may be worked out by solving the Schrodinger

equation [4,21]. There are also methods for the calculation of the band structure of the solid from first principles.

Electrons in the conduction band and holes in the valence band behave as free particles, and their distribution among the available energy levels, when in thermal equilibrium with the lattice, obeys Fermi-Dirac statistics. For the parabolic band, the number of electrons occupying a particular energy level is given by

$$n = 4\pi\left(\frac{2m^*}{h^2}\right)^{3/2}\int_0^{\infty}\frac{E^{1/2}dE}{1+\exp\left(E-E_f\right)/k_bT} \tag{2.19}$$

where, h is the Planck's constant and k_b is the Boltzmann constant. The density of states in the energy space varies as $E^{1/2}$.

Integral in Equation (2.19), in general, cannot be evaluated analytically. But when E_F is negative and $|E_F|$ is much larger than k_bT, i.e. when the material is non-degenerate, the Fermi function simplifies to the Maxwellian function. Then, by neglecting 1 in comparison to $\exp[(E - E_F)/k_bT]$, we get

$$n=2\left(\frac{2\pi m^* k_bT}{h^2}\right)^{3/2}\exp(E_F/k_bT)=N_c\exp(E_F/k_bT) \tag{2.20}$$

But, in the degenerate case, when E_F is positive and is not much lower than k_bT of band edge, the integral has to be evaluated numerically. The integral in Equation (2.19), can be written as

$$n=N_C\frac{2}{\sqrt{\pi}}\int_0^{\infty}\frac{x^{1/2}}{1+\exp(x-\eta)}=N_C F_{1/2}(\eta) \tag{2.21}$$

The integral in the above form is often called Fermi integrals, where $x = E/k_bT$ and $\eta= E_F/k_bT$. The distribution function F_i is called the "Fermi-Dirac Distribution" function [8] and is defined for any index i as

$$F_i=F_i(\eta)=\int_0^{\infty}\frac{x^i dx}{1+\exp(x-\eta)} \tag{2.22}$$

From Equations (2.19) and (2.21), we can relate the concentration of electrons to the Fermi energy and to the density of states. Later, we can determine the position of the Fermi level for different impurity concentrations and temperature.

2.2.1.2 Electron Scattering The motion of an electron is unhampered in a perfect crystal, in which the wave function of the electron is given by stationary Bloch functions, and the application of an external field would uniformly accelerate the electron causing a linear increase in the drift velocity with time in the direction of the field. But such linear increase in drift velocity with time does not occur in real crystals. The average drift velocity of the electron reaches a limiting value, which, at low field, will be proportional to the magnitude of the field. The limit is set by the interaction of the electron with the imperfection of the crystal through the process referred as scattering or collision processes. The electron continues to be in a stationary state until it comes close to an imperfection. After it interacts with the imperfection, the electron has a new wave function characterized by new wave vector and often different value of energy [23].

In a lattice crystal, there are different types of scattering mechanisms for different imperfections. The importance of each kind of scattering varies from material to material; it also depends on temperature and carrier concentrations. Later, we will discuss the importance of electron scattering mechanism for Si, Ge, and SiGe alloys. In the Figure 2.11, below, we present a list of electron scattering mechanisms.

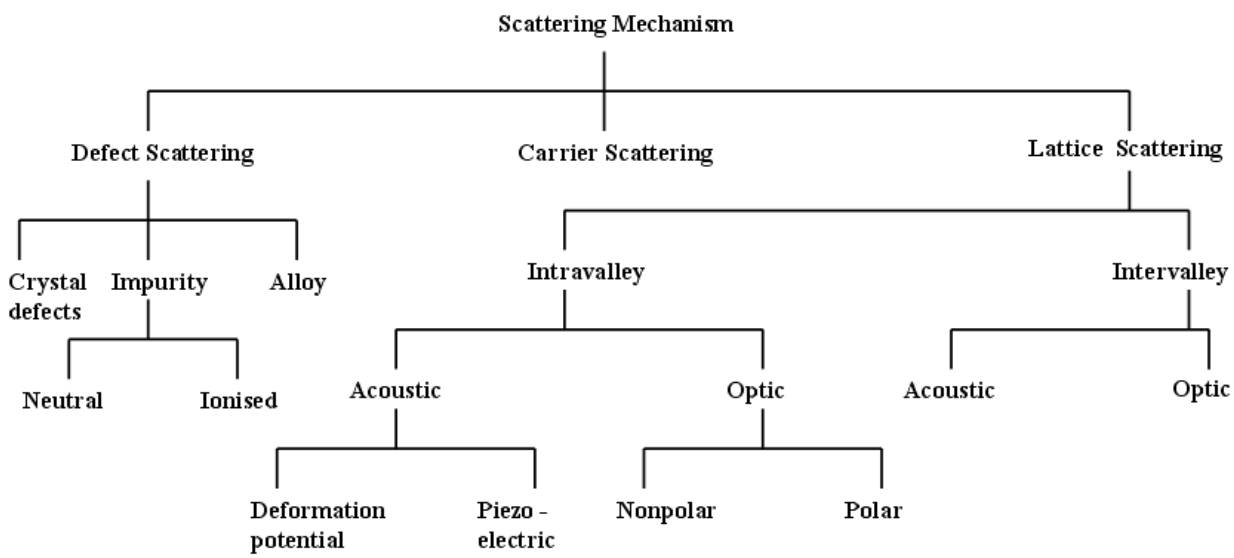

Figure 2.11 Electron scattering Mechanisms.

Source: Chandan Bera. Thermoelectric properties of nanocomposite materials. Engineering Sciences. Ecole Centrale Paris, 2010. English. <NNT: 2010ECAP0027>.

2.2.1.3 Kinetic Theory of Electron Transport After having defined the scattering mechanisms for different kinds of materials, we have to know the different macroscopic transport coefficients to calculate the transport properties of the material. In the simplest kinetic method, we can define some macroscopic properties of materials by considering electron as a particle and following the motion of each of them at a time. Here, the

particle scattering is governed by the characteristic relaxation time τ when a particle collides with impurities or interacts with phonons. For n electron per unit volume, we can define the electric current as,

$$J = ne\overline{\delta v} = \frac{ne^2 v\tau}{\delta E/\delta v} E \tag{2.23}$$

where, $\overline{\delta v}$ is the average drift velocity parallel to the Electric field E. Now, the macroscopic relation defining the electrical conductivity, **σ**, in Equation (2.23) becomes,

$$J = \boldsymbol{\sigma} E \tag{2.24}$$

Therefore,

$$\boldsymbol{\sigma} = \frac{ne^2 v\tau}{\delta E/\delta v} = \frac{ne^2 \tau}{m^*} \tag{2.25}$$

In terms of electron mean free path, l_e, where $l_e = \tau v$, the electrical conductivity becomes,

$$\boldsymbol{\sigma} = \frac{ne^2 l_e}{m^* v} \tag{2.26}$$

We can also relate the mobility (μ) of the material with the relaxation time and the carrier concentration, n as,

$$\mu = \frac{e\tau}{m^*} \tag{2.27}$$

because $\boldsymbol{\sigma} = ne\mu$

2.2.2 Phonon Transport in Bulk Materials

In solid materials, heat is transported by the atomic lattice vibration, called phonons and charge carriers such as electrons and holes. The contribution of charge carriers in heat transport was discussed in the earlier section. The electronic contribution explains the fact that good electrical conductors also have high thermal conductivity. Although electronic contribution in thermal conductivity is significant for highly doped materials and metals, the lattice contribution remains dominant in dielectrics and semiconductor materials.

2.2.2.1 Phonon Dispersion Curves Atoms in solids are held together as a lattice by a chemical bond between them. These bonds are not rigid, but act like a spring which connects the atoms, by creating a spring-mass system as shown in Fig. 2.13. When an atom or plane of atoms displace, this displacement can travel as a wave through the crystal, transporting energy as it propagates [23]. This wave can be longitudinal where the displacement of atoms is in the same direction of wave, or they can be transverse where, in the three dimensional case, the displacement of atoms is in the direction perpendicular to the wave propagation. These lattice vibrations are quantized and known as phonons.

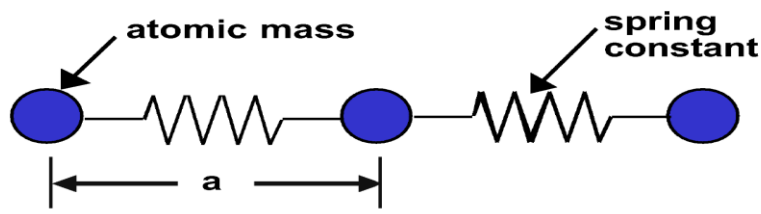

Figure 2.12 One dimensional representation of atoms and chemical bond as spring mass system. The chemical bond acts as a spring and atom as mass. The distance between the two adjacent atoms is called lattice constant and is represented by a.

Source: Chandan Bera. Thermoelectric properties of nanocomposite materials. Engineering Sciences. Ecole Centrale Paris, 2010. English. <NNT: 2010ECAP0027>.

By solving the equation of motion for these waves, we can determine the angular frequency of the waves (ω) for its different wavelength (λ) or wave number (also called wave vector) (k), where k = 2л/λ. The relationship between k and ω is called the "Dispersion Relation". From the slope of the dispersion relation, one can determine the speed of propagation of phonons, ($\frac{\delta\omega_k}{\delta k}$), which is also called "Group Velocity". For a crystal that has at least two atoms in a unit cell (which may or may not be different), the dispersion relations exhibit two types of phonons, namely, optical and acoustic modes corresponding to the upper and lower sets of curves in Figure 2.14, respectively. The vertical axis is the energy or frequency of phonons, while the horizontal axis is the wave-vector. [20]

Since the group velocity of the acoustic phonons is much larger than the one of optical phonons, the contribution to the thermal conductivity is mostly from acoustic branch.

2.2.2.2 Phonon Energy As the dispersion relation of the phonon is known, one can determine the thermal properties of solid from there. The entire set of all possible phonons that are described by the above phonon dispersion relations combine in what is known as the phonon density of states which determines the heat capacity of a crystal. We consider the solid as an assembly of 3 NV independent harmonic oscillators, one for each lattice mode, which is capable of taking up one or more quanta of energy. Therefore, phonons are 'Bose-Einstein particles' [8] of which any number may go to any given energy level. The equilibrium number of phonons with a polarization ‘p’ and wave vector ‘k’ is given by

$$\langle n_{k,p} \rangle = \frac{1}{\exp\left(\frac{\hbar\omega}{k_b T}\right) - 1} \tag{2.28}$$

where, k_b is the Boltzmann constant, and T is the temperature.

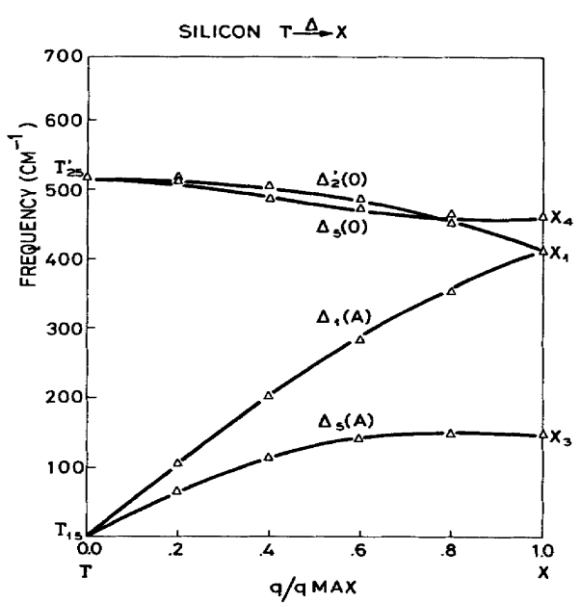

Figure 2.13 Dispersion Relation of Phonons.

Source: Riccardo Tubino. Lattice dynamics and spectroscopic properties by a valence force potential of diamond like crystals: C, SiGe, and Sn. The Journal of Chemical Physics, 56(3):1022, 1972.

The average energy of this mode is [22]

$$E=\sum_p \sum_k (< n_{k,p} > + \frac{1}{2})\, \hbar\omega \qquad (2.29)$$

Crystal volume energy, E is obtained by summarizing each quanta $\hbar\omega$ over the two polarizations of phonon for longitudinal and transverse component of acoustic and optical modes. Assuming that phonon wave vector k is sufficiently dense in K space, the summation over k may be replaced by an integral [23],

$$E=\sum_p \int_\omega (< n_{k,p} > + \frac{1}{2})\hbar\omega D_p(\omega) g_p d\omega \qquad (2.30)$$

where, $D_p(\omega)d\omega$ is the number of vibrational modes in the frequency range $[\omega, \omega+, d\omega]$ for polarization p and g_p is the degeneracy of the considered branch.

2.2.2.2 Phonon Scattering When different kinds of phonon waves propagate through the lattice, they are disrupted or scattered by the defects or dislocations, crystal boundary, impurities such as dopant or alloying components, or by interaction with other phonons [12,24]. These different types of scattering can be divided in two groups, one elastic scattering where the frequency does not change after the scattering and another inelastic scattering where frequency changes after the scattering.

The distance or the path traveled by phonons between two scattering event is generally defined by the phonon mean free path l_p, where

$$l_p = v\tau \tag{2.31}$$

v is the phonon velocity and τ is the relaxation time of the scattering events. Each scattering event has its own mean free path which depends on the materials and the temperature.

1. Normal and Umklapp Scattering. Inelastic scattering process arises due to the fact that forces between atoms are not purely harmonic. There are two types of phonon-phonon scattering, one is Normal and another is Umklapp which are generally referred as N and U scattering process. Normal scattering process is shown in Figure 2.15.

   Here, two phonons K_1 and K_2 interact with each other and produce another phonon K_3 or one phonon can be scattered into two phonons. In this scattering mechanism, the phonon momentum does not change; so it does not put any resistance in the heat transport.

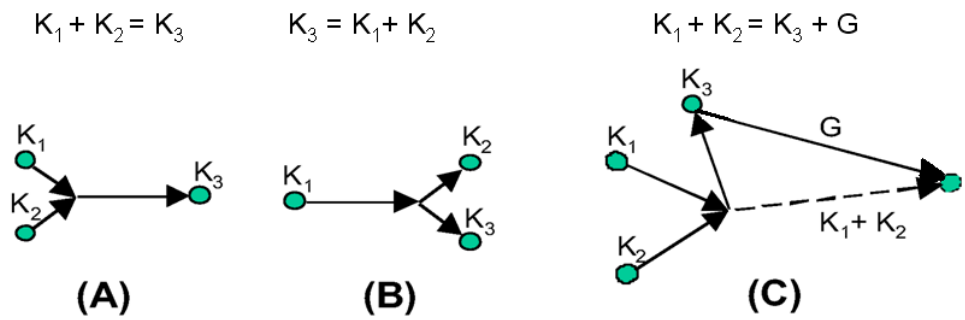

Figure 2.14 (a) Vectorial representation of a normal phonon scattering where two phonons combine to create a third. (b) Normal processes where one phonon scatters into two phonons. (c) Umklapp processes where two phonons combine to create a third. Due to the discrete nature of the atomic lattice, there is a minimum phonon wavelength, which corresponds to a maximum allowable wave vector. If two phonons combine to create a third phonon which has wave vector greater than this maximum, the direction of the phonon will be reversed with a reciprocal lattice vector G, such that its wave vector is allowed.

Source: Scott Thomas Huxtable. Heat transport in super-lattices and nanowire arrays. University of California, Berkeley, 2002.

The Umklapp phonon scattering mechanism is described in Figure 2.14(c), where, after the scattering, new phonons may cross the first Brillouin zone and the momentum direction after the scattering is changed. Umklapp scattering is the dominant process for thermal resistivity at high temperatures for low defect crystals [12, 25].

2. Scattering by defects, impurities, and boundary. In addition to phonon-phonon interaction, there may be phonon scattering by the imperfections in the crystal lattice. This imperfection may be due to the defects in the crystal, or due to impurities and the boundary of the crystal. In the crystal lattice, imperfection occurs due to various reasons. All kinds of imperfections mostly have the same effect, i.e. reducing heat transport. The types of defects are classified as isolated

point imperfections (i.e., vacancies, chemical impurities, isotopes), line imperfection (typically dislocation), surface of imperfection, e.g., grain boundaries, twin boundaries and stacking faults and volume disorder as in the case of alloys [12,24]. Defects or dislocations in the atomic lattice have the effect as acting as different springs and mass constants to the incident phonon. The speed of sound related to the elastic stiffness(C) of the chemical bond is defined by the bellowing equation,

$$v=\sqrt{\frac{c}{\rho}} \tag{2.32}$$

where, ρ is the mass density and v is the speed of sound. So when a phonon encounters a change in mass or elastic stiffness, it is scattered. The impurity atoms inside the host matrix with different mass and spring constant produce a disruption in the phonon transport. These impurity atoms can be in the form of dopant atoms or from the species introduced to form an alloy [12]. Alloying is a very effective way to reduce thermal conductivity due to this kind of scattering.

The role of boundary scattering in limiting the phonon mean free path has long been considered as low temperature phenomena. In the absence of other phonon scattering mechanism, boundary scattering can be observed as phonon mean free path approaches the sample dimensions [26]. In recent years, interest has grown in the use of hot-pressed highly doped materials in thermoelectric applications. There are significant contributions from boundary scattering as, in the solid, large proportion of heat is carried

by low frequency phonons; boundary scattering effects can manifest themselves at high temperatures [12,27].

2.2.2.4 Phonon Thermal Conductivity In the kinetic formulation of thermal conduction, we can define the heat flux, $\overline{q}$ as equal to the product of thermal conductivity, k and the negative local temperature gradient, -∇T. The heat flux is the amount of energy that flows through a particular surface per unit area per unit time. The final relation is also called "Fourier's Law" of thermal conduction.

$$\bar{q} = -k \times \nabla T \tag{2.33}$$

Now, we suppose that each particle has an atomic heat capacity c, so that it requires an energy c δT per particle to change the local temperature of the assembly by an amount δT and each particle is traveling with a velocity v from one region to another region. If the motion of one particle is unrestricted for a time t, the contribution of this particle to the thermal current per unit area, $\bar{q}$, will depend on the distance vt that it crosses before it is scattered. The average value of this over the particle is vT, where T is the relaxation time. Summing over all the particles, we can write the heat current as [28]

$$\bar{q} = -nc\tau\overline{v^2}.\nabla T \tag{2.34}$$

where, n is the total number of particles. Now the thermal conductivity, k, is

$$k = \frac{1}{3} C_p \bar{v}\, l_p \tag{2.35}$$

since $\bar{v}$ corresponds to the total specific heat C_p, and l_p is given by Equation (2.31).

From Equations (2.26) and (2.35), we can calculate very easily some important properties of the material. From these two equations, we can also calculate the mean free path of the carriers without knowing details of the scattering mechanisms. By assuming $l_e = l_p$ we can write,

$$\frac{k}{\sigma} = \frac{c_p\, m^* v^2}{3ne^2} \tag{2.36}$$

For the classical gas, where $\frac{1}{2}mv^2 = \frac{3}{2} k_b T$ and the specific heat is $\frac{3}{2} nk_b$, Equation (2.36) becomes [8, 29]

$$\frac{k}{\sigma} = \frac{3}{2}\left(\frac{k_b}{e}\right)^2 T \tag{2.37}$$

The ratio $k/\sigma T$ is called the "Lorenz Number" and should be a constant, independent of temperature as well as the scattering mechanisms. Equation (2.37) is in fact the well-known as "Wiedemann-Franz Law" [28].

Understanding when the Wiedemann-Franz relation fails is extremely important for research in thermoelectrics. This is due to its general use to calculate the electronic thermal conductivity in order to deduce the lattice thermal conductivity from the

experimentally measured total thermal conductivity. Reducing the lattice thermal conductivity to its minimum value is one approach to improving the overall performance of thermoelectric materials [30-32].

CHAPTER 3

FIGURE OF MERIT (ZT)

The best thermoelectric materials were succinctly defined as ‘‘phonon-glass electron-crystals’’ (or PGEC in short), which means that the materials should have a low lattice thermal conductivity as in a glass, and a high electrical conductivity as in a crystal [33]. The interdependency of the TE parameters makes the enhancement efforts of ***ZT*** very challenging. The normal ways of optimizing TE materials are to increase the power factor $S^2\sigma$ by optimizing the carrier concentration ‘n’, and / or to reduce the lattice thermal conductivity K_L by introducing the scattering centers. These parameters are function of scattering factor ‘r’, carrier effective mass m* and carrier mobility m and their interconnectivity limit ***ZT*** to about 1 in large bulk materials.

According to the kinetic energy definition, S is the energy difference between the average energy of mobile carrier and the Fermi energy [34]. If the carrier concentration n is increased, the Fermi energy as well as the average energy increases. However, the Fermi energy increases more rapidly than the average energy when n is increased. As a result, S decreases, lowering the power factor (S2n) rapidly. Thus, in attempting to increase ***ZT*** for most of the homogeneous materials, the carrier concentration (n) increases the electrical conductivity (σ) but reduces the Seebeck coefficient (S).

For this reason, in metals and degenerate semiconductors (energy-independent scattering approximation), the Seebeck coefficient can be expressed as [35]

$$S=\frac{8\pi^2 k_B^2}{3eh^2}\, m^*T \left(\frac{\pi}{3n}\right)^{2/3} \qquad (3.1)$$

The parameter m* is the density of states effective mass in Equation (3.1). The high m* influences the power factor to raise according to the Equation (3.1). Most materials having high m* have generally low m which limits the power factor by a weighted mobility with the relationship of power factor proportional to $(m^*)^{3/2}\mu$.

It should also be noted that the defects scatter not only the phonons but also the electrons. Hence there are some trade-offs carried out in carrier mobility when designing thermoelectrics by reducing the lattice thermal conductivity. The ratio of μ/K_L determines the improvement in ***ZT*** [36].

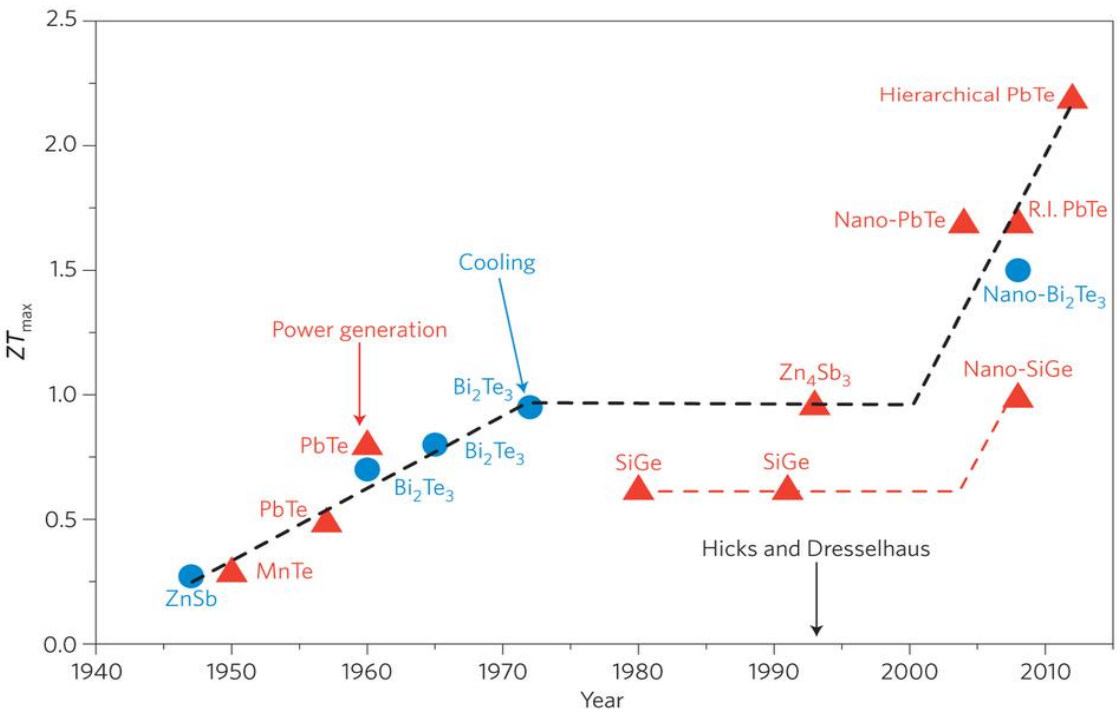

Figure 3.1 Evolution of Maximum ***ZT*** over Time

Source: Joseph P. Heremans, Mildred S. Dresselhaus, Lon E. Bell & Donald T. Morelli, When thermoelectrics reached the nanoscale, *Nature Nanotechnology*, 8,471–473(2013) /nnano.2013.129

3.1 Strategies to Enhance ZT with Novel Approaches

A renewed interest in thermoelectrics began in 1990's after the four decade of slowdown in research. Novel approaches opened several possibilities to enhance ***ZT***. One of the widely adopted methods to enhance ***ZT*** is to reduce the lattice thermal conductivity. Three general approaches are mainly used to reduce the thermal conductivity. In one approach, phonon scattering is used to reduce the thermal conductivity. It can be achieved by scattering phonons in different frequency ranges utilizing a variety of methods such as mass fluctuation scattering (a mixed crystal in ternary and quaternary compounds), grain boundary scattering due to the size of the grains and interface scattering in thin films or multilayer systems [37].

In the second approach to reduce thermal conductivity, complex crystal structures were used to separate the electron crystal from the phonon glass. In the third method, multiphase composites were mixed on low dimensional materials to increase scattering [38].

3.2 Nanostructured Thermoelectric Materials

Low dimensional materials were used either to enhance the power factor or to reduce the lattice thermal conductivity. In one approach, the nanoscale constituents are used to introduce quantum confinement effects to increase power factors. In the second approach, the nanostructures introduce many internal interfaces to scatter phonons. The enhancement in the density of states near E_f leads to higher Seebeck coefficient. With low dimensional materials, it is advantageous with anisotropic Fermi surfaces in multi valley cubic semiconductors and increased mobilities at a given carrier concentration

when the quantum confinements are satisfied so that modulation doping and delta doping can be utilized. Thus, this makes it easy to manipulate the thermoelectric parameters. The other aspect is that low dimensional particles are promising candidates in increasing ZT also because Wiedmann Franz law is not applicable to nano-materials with delta like DOS [39]. The carrier mobility m is independent of electron– phonon coupling under normal conditions such as near and above room temperature [40]. Hence, phonon drag has been ignored in most of the calculations in these temperature ranges [41].

Theoretical predictions on strong enhancements in ***ZT*** is based on the modification of K_e and power factor due to the spatial confinement of carriers and corresponding change in carrier density of states. These predictions generally ignored spatial confinement of phonons and used bulk values of K_{ph}. The phonon confinement affects the entire phonon relaxation rate and this makes difference in the thermal transport properties of nanostructures from bulk structures. The change in phonon group velocities and dispersion, due to spatial confinement, leads to the increase in the phonon relaxation rate and strong drop in lattice thermal conductivity. ***ZT*** was simulated to show more increase than its bulk/ ingot counterpart at this condition [41].

Energy barrier filtering and high electron density in metals produce large moment of differential conductivity about the Fermi level. Also high interface density, large mismatch in phonon density of states and electron–phonon interface resistance suppress thermal conductivity. If nanoscale roughness can be designed to overcome the constraints of parallel momentum conservation, very high ***ZT*** may be possible [42].

The thermal conductivity of pressure sintered $Si_{80}Ge_{20}$ alloy is less than that of crystalline alloy because of the point defects. However, ***ZT*** is not increased due to the

proportional reduction in electrical conductivity. Similar results were obtained with Si/Ge superlattice, $Si_yGe_{1-y}/Si_xGe_{1-x}$ superlattice, where the reduction in thermal conductivity did not increase ***ZT*** [43].

Table 3.1. Material Properties of SiGe and Si

Materials [76,77]	Type	Seebeck Coefficient (μV/K)	Resistivity (μOhm-m)	Conductiv--ity (W/mK)	ZT (10^{-3}/K)	Doping Concentration (10^{20}/cm^3)
Poly SiGe	n type	-136	10.1	4.45	0.328	1-3
	p type	144	13.2	4.80	0.413	2-4
Poly Si	n type	-120	8.5	24	0.017	3.4
	p type	190	58	17	0.037	1.6

Source: Hilaal Alam, Seeram Ramakrishna, A review on the enhancement of figure of merit from bulk to nano-thermoelectric materials, Oct-2012, pp 203.

3.3 Future Research in Nanocomposites

Si being abundant and the most widely used semiconductor, Si-based nanocomposites, in thin film form, is expected to grow and contribute to improve the thermal management in microelectronics and related industries. The main advantage of using Si nanowires for thermoelectric applications lies in the large difference in mean free path lengths between electrons and phonons at room temperature [44].

By using roughened silicon nanowires, the thermal conductivity has been reduced to ~1.6 W/mK, with the phonon contribution close to the amorphous limit, with not much

compromise on power factor so that ***ZT*** has been achieved to near unity at room temperature. Instead of random nanocomposites, ordered nanocomposites have proven to be better and hence have good potential as thermoelectrics. It is still not understood clearly as to which carriers are dominant heat/charge carrier, what the optimal size distribution is and the type of interfaces that lead to strong phonon scattering and weak electrons [45].

Energy filtering techniques are used to filter phonons and allow high energy electrons to pass through. This increases the Seebeck coefficient due to the negative Seebeck distribution. However, it will not be simple to filter energy by merely controlling the grain boundaries as it is related to the electron mobility. The mobility of electrons through the grain in n type $Si_{80}Ge_{20}$, for example, decreases by 40% in the experimental results compared to the theoretical calculations. The density of states can be increased by introducing energy levels that are created by impurities. Due to these impurities, the energy levels lie in the conduction or valence bands creating the resonant level and a local maximum in the electronic density of states [46].

CHAPTER 4

SiGe- AS THERMOELECTRIC MATERIAL

In this section, the overview of SiGe as thermoelectric materials and the associated properties are illustrated.

4.1 Material Introduction

Russian scientist Abram Ioffe demonstrated the promise of semiconductors for thermoelectric applications in 1929 [47]; see Figure 4.1.

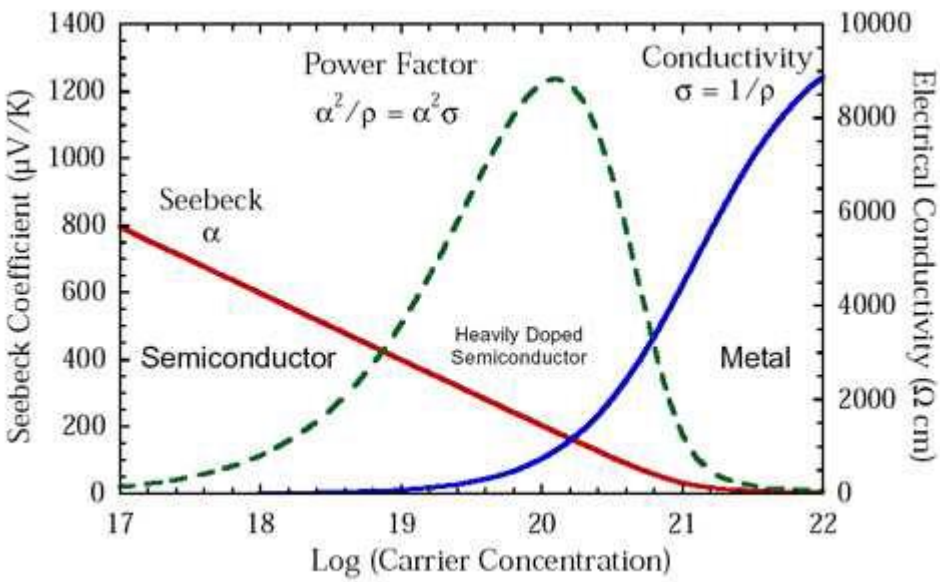

Figure 4.1 Electrical conductivity and Seebeck Coefficient plotted versus carrier concentration.

Source: J. Snyder. Thermoelectrics. http://www.its.caltech.edu/~jsnyder, Dec 2014.

In early 1930's, synthetic semiconductors, with high Seebeck coefficient, were introduced. By 1954, H.J. Goldsmid and R.W. Douglas expanded Ioffe's work, and further advances in the field of semiconductor technology attracted much attention to the

field of thermoelectrics. Specifically, RCA Laboratories, spurred by the U.S. Navy, began active research into thermoelectric materials because of their potential military applications [48]. This led to the discovery of SiGe as a thermoelectric material in the late 1950's [49]. Since this time, SiGe has become the established material for high temperature power generation applications. In going over modern day ***ZT*** values and other related properties, one sees that SiGe is still the preferred material for its temperature regime, as shown in Figure 4.2. The obvious advantage over other high temperature materials is that SiGe has both a p-type and n-type material.

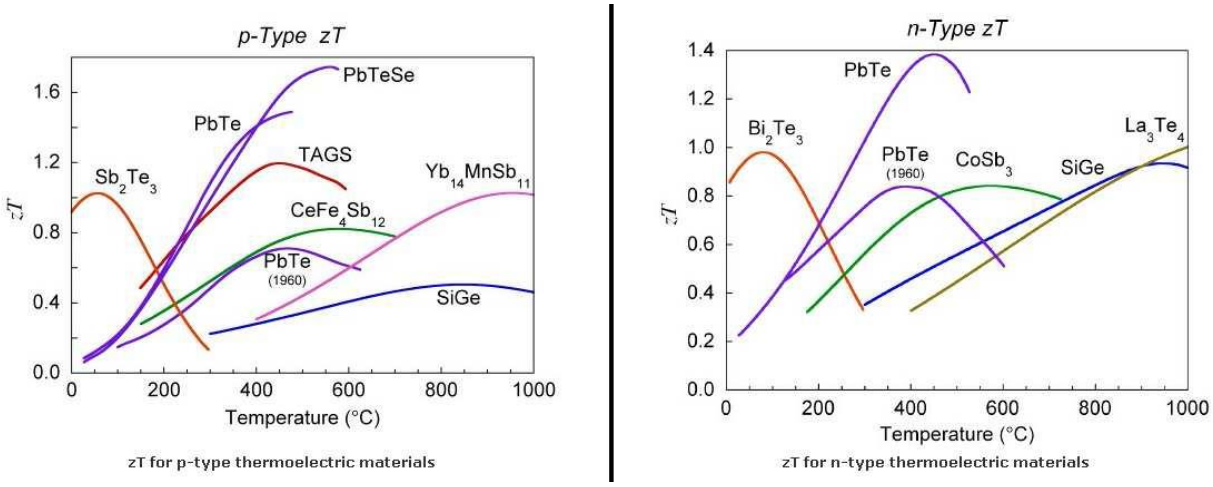

Figure 4.2 Modern day ZT values.

Source: G. Snyder and E. Toberer. Novel thermoelectric materials. *Nature Materials*, 7:105–114, 2008.

4.2 History of Thermoelectric SiGe Alloys

The potential of silicon-germanium solid solutions as a thermoelectric was shown in 1958 by Steele and Rosi [49]. In 1964, Dismukes et al. provided the foundation for future optimizations with their work on silicon-rich SiGe alloys [50]. Although carried out for the U.S. Navy, this work was later employed by NASA on Radioisotope Thermoelectric

Generators (RTGs) operating from 600 − 1000°C which was very useful for space missions [48,51]. Specifically, SiGe alloys, synthesized by the time consuming zone leveling process, were first used on the 1965 NASA SNAP-10 mission.

In the late 1960's, grain boundary scattering and the use of fine-grained alloys in order to lower lattice thermal conductivity were studied for SiGe [52,53]. This led to D.M. Rowe's study of the grain size effect on thermal conductivity [54]. In the mid-1970's, Sandia Laboratories published a three part review on the synthesis of SiGe materials by the chill casting method. Other investigations during the 1970's, included various milling, sintering, and pressing techniques [55,56]. By 1976, SiGe had become the sole material used in RTGs for all deep space power generation applications [48]. The 1980's saw diminished interest in all thermoelectrics research. Although the general interest for thermoelectrics was boosted by superconductors, for SiGe, interest was renewed in the late 1980's, when NASA was considering other power sources for their deep space missions. This led to a large body of research on SiGe during this period. It was found that, in spite the promise of other advanced materials when it came to providing power, SiGe alloys remained the material of choice due to their robust nature [57]. In 1987, Vanersande et al., at the Jet Propulsion Laboratory(JPL), found that n-type SiGe/GaP samples had a ***Z*** value about 20-30% greater than zone leveled or hot-pressed n-type SiGe [58]. In 1989, work done by Bruce Cook at Ames laboratory introduced mechanical alloying, as opposed to zone leveling, as a simpler way to synthesize SiGe alloys [59]. In the 1990's, Cook continued to optimize his mechanical alloying (MA) method using SPEX mills [60-63]. MA is a high energy ball mill process. Essentially, powders/specimens are loaded into robust vials filled with one to several balls. For

milling SiGe materials, these vials and balls are made of hardened steel. The vials are then placed in a specialized shaker. The striking of the balls against the sides of the vial allows for the repeated fracturing and cold welding of the materials resulting in a fine alloyed powder. The optimization of MA by Cook led to his thorough investigation of the parasitic effects that oxygen has on n-type $Si_{80}Ge_{20}$ thermoelectrics (GaP and P doped) [60, 61].

The new millennium witnessed a study of super-lattices with quantum dot super-lattices (QDS) and nano-dot super-lattices (NDSLs) [64-66]. Even through the nanophase, the new theoretical limit was achieved in the 1990's; the high performance SiGe alloys used in modern space missions have a figure of merit of $\boldsymbol{ZT}\approx 0.50$ (p-type) and $\boldsymbol{ZT}\approx 0.93$ (n-type). The values of $\boldsymbol{ZT}$ for modern RTG SiGe are lower than that of the nano-phase theoretical limit due to the ability to mass produce perfectly doped alloys. Also, these values are lower than the current nano-structure SiGe materials, but super-lattice SiGe is not presently capable of being produced in bulk.

4.3 Properties of p-,n-Type $Si_{80}G_{20}$

The thermoelectric transport and other general properties of both n-type and p-type $Si_{80}Ge_{20}$ can be found in the 1995 edition of the thermoelectrics handbook [66]. Another useful source of information is the "New Semiconductor Materials Website" [67]. The fastest measurement that can be performed to see if a material is both a good thermoelectric and the correct alloy is by checking its theoretical density. The theoretical density is composition dependent for the alloy, as given by Equation (4.1). Thus, for $Si_{80}Ge_{20}$, the theoretical density is 3.00 g/cc [67].

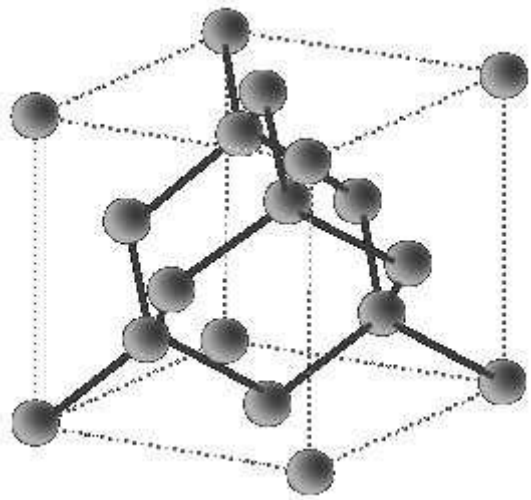

Figure 4.3 Sample of Si/Ge crystal structure.

Source: Vadim Siklitsky. Silicon germanium. http://www.ioffe.rssi.ru, May 2012. (Accessed: 21/02/2015)

$$Si_{1-x}Ge_x \text{ (g/cc)} = (2.329 + 3.493x - 0.499x^2) \quad (4.1)$$

Beyond the density, another important property to consider is the crystal structure of SiGe alloys. SiGe has a diamond lattice (space group Fd3m) consisting of two inter penetrating face centered cubic primitive lattices; see Figure 4.3. Similar to the density, the lattice constant is composition dependent. This idea (Vegard's law) that a linear relation exists between the crystal lattice parameter of an alloy and the concentration of its constituent elements was proposed by Vegard in 1921 [50,68]. Dismukes formulated the slight variation from Vegard's law for SiGe alloys in 1964, as in Equation (4.2) [50, 69]. This formulation will become invaluable for demonstrating that the Single–Element Spark Plasma Sintering (SE SPS) is truly alloying different compositions of SiGe.

$$Si_{1-x}Ge_x \text{ (Å)} = (5.431 + 0.20x + 0.027x^2) \text{ (Å) at 300K} \quad (4.2)$$

The specific heat of a material is usually quite robust, not easily changed by small variations in composition or dopants. Therefore, it is not surprising that the specific heat for SiGe alloys is virtually the same for the n-type and p-type material; see Figure 4.4.

When it comes to the thermoelectric properties of a material, there are the measurable bulk transport properties, σ, α, and κ, and the more fundamental transport properties such as carrier concentration, n, and mobility, μ. Since synthesis techniques and dopant concentrations can have a large effect on n and μ, one should refer directly to the reference handbook or Vining's review paper for acceptable values of these parameters for thermoelectric SiGe [48,50,70]. The bulk transport properties provided by tables in the reference handbook are plotted below; see Figures 4.4, 4.5, and 4.6.

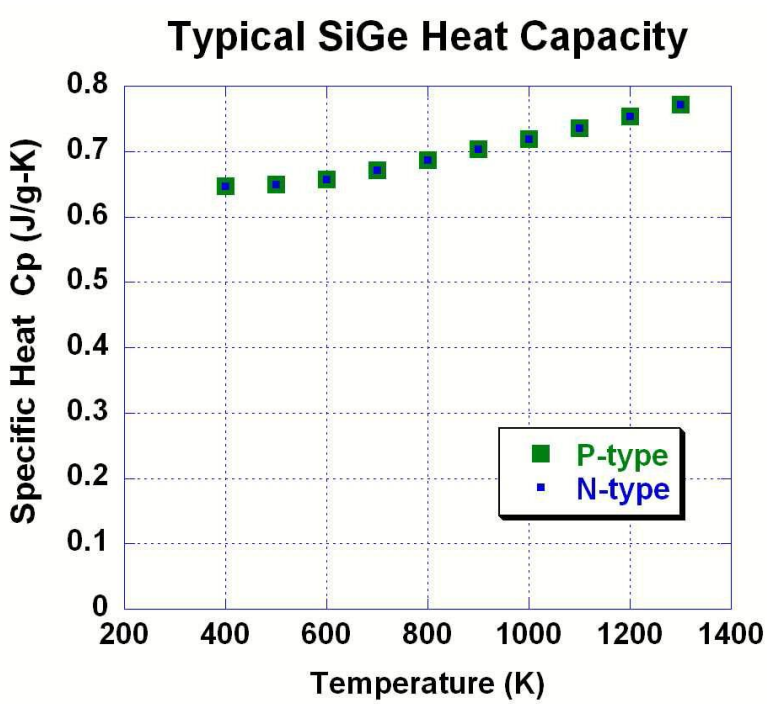

Figure 4.4 The specific heat of typical thermoelectric SiGe.

Source: D.M. Rowe. *CRC Handbook on Thermoelectrics*. CRC Press, 1995

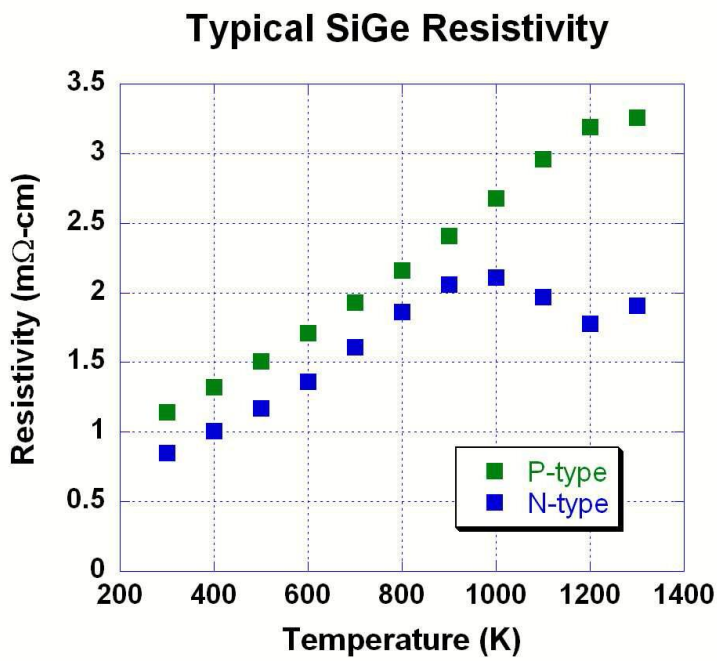

Figure 4.5 The resistivity of typical thermoelectric SiGe.

Source: D.M. Rowe. *CRC Handbook on Thermoelectrics*. CRC Press, 1995

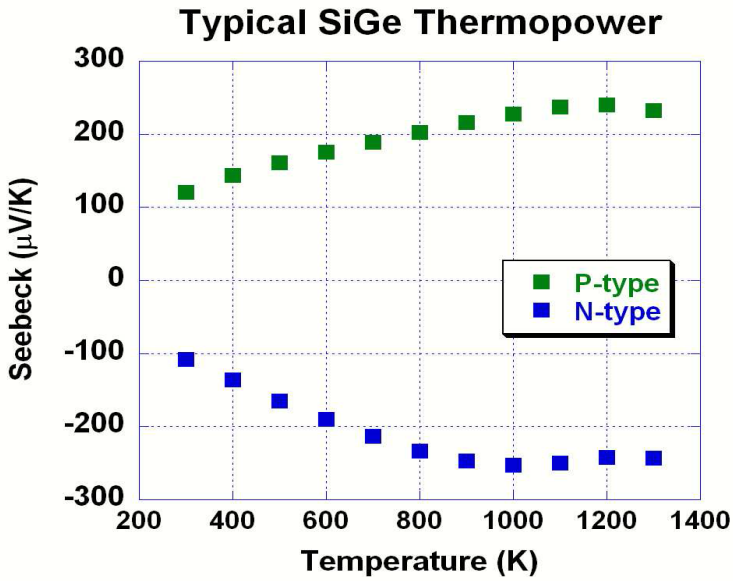

Figure 4.6 The thermopower of typical thermoelectric SiGe.

Source : D.M. Rowe. *CRC Handbook on Thermoelectrics*. CRC Press, 1995

These properties can be combined to form the dimensionless figure of merit. As for most thermoelectric materials, ***ZT*** for n-type is greater than that of the p-type, as in Figure 4. 7.

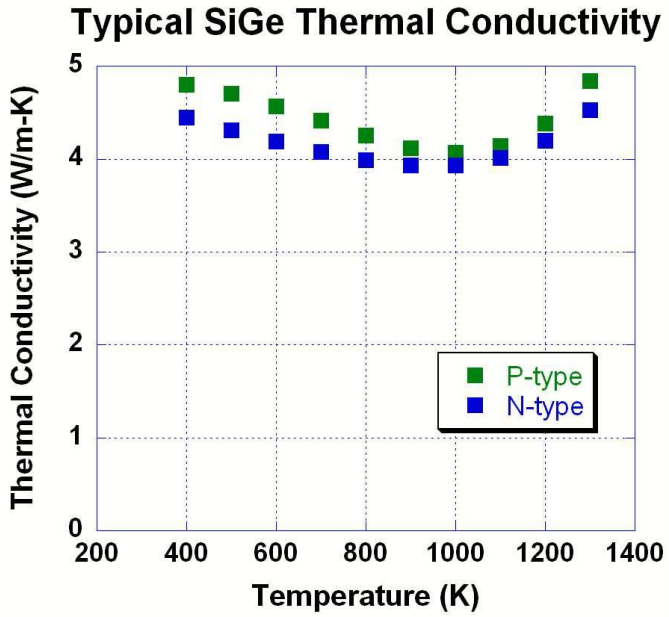

Figure 4.7 The total thermal conductivity of typical thermoelectric SiGe.

Source: D.M. Rowe. *CRC Handbook on Thermoelectrics*. CRC Press, 1995

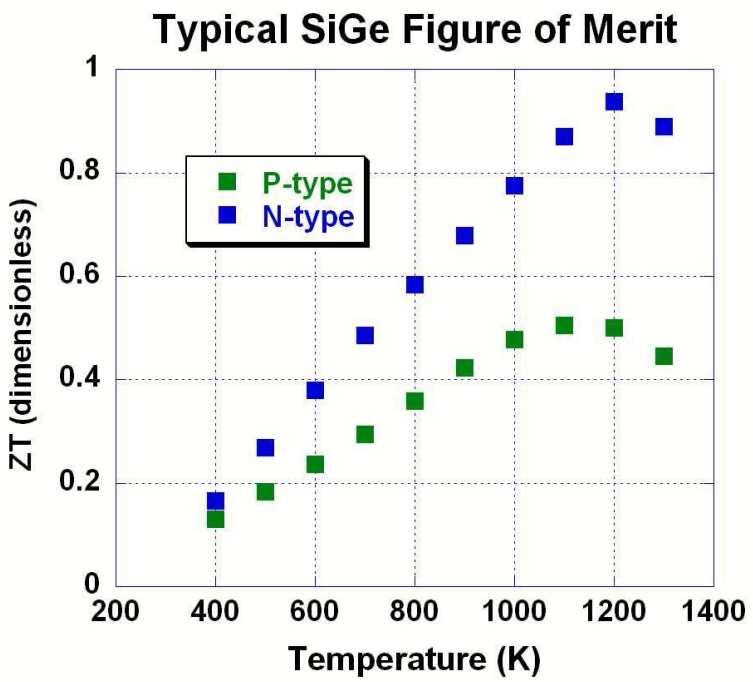

Figure 4.8 The ZT of typical thermoelectric SiGe.

Source: D.M. Rowe. *CRC Handbook on Thermoelectrics*. CRC Press, 1995

4.4 Recent Advances in SiGe Alloys

In 2008, collaborative work between Boston College, MIT, and GMZ Energy produced nano-structured SiGe bulk alloys via MA that avoided past problems with oxidation and showed that nano-structures can be successfully incorporated. They reported ***ZT*** values of ***ZT***=0.95 (p-type) and ***ZT***=1.3 (n-type) [71, 72]. This work opened the door for examining whether the reduction in lattice thermal conductivity arose in the alloy through scattering by point defects, or from the nano-size effects by the strong interface scattering of phonons. Previous studies, before this one, were unable to differentiate between the two causes for phonon scattering [73]. The success of bulk nano-structure SiGe led to further theories on the maximum obtainable ***ZT*** for this material with nano-phases [74].

During this time, others within the MIT collaborating team began to investigate the viability of ultra-low content SiGe alloys with the bulk nano-composite approach. Essentially this work showed the tradeoff between traditional $Si_{80}Ge_{20}$ with an average ***ZT*** of 0.49 at a cost of $9/Watt and nano-structured $Si_{98}Ge_{02}$ with an average ***ZT*** of 0.32 at a cost of $1.7/Watt. This approach provides a tradeoff of the material's overall performance (Watt/mass) with its economic cost (Dollar/Watt) [75]. The reason that this cost per watt is significant for thermoelectric materials is because lower economic cost enhances the applicability of these materials beyond their current niche markets. Often, certain cost per watt goals are set by the DOE, such as for solar cells that have a goal of $1/Watt [76].

Further improvements to bulk nano-structured SiGe alloys were recently shown by the MIT group. These improvements relied on modulation doping (adding an additional Si phase) [77]. This idea will be revisited in suggestions for future work, and the SE SPS method has potential for modulation doping to further improve the ***ZT*** of the materials it alloys. These recent advances in SiGe from the MIT collaborations involve a large group of researchers that includes Mildred Dresselhaus and those who worked on SiGe at the Jet Propulsion Laboratory in the 1990's. Therefore, it is essential for anyone interested in SiGe alloys to pay close attention to their work, since their research arises from well-established experimentalists and theorists that are experts in this material and field [50].

CHAPTER 5

PROPERTY MODELING

Although the nanocomposite approach is one of the most cost-efficient ways to produce thermoelectric materials with high ***ZT*** values [78-80], there have been only a few modeling studies on transport phenomena in such nanocomposites. Thermal conductivity is relatively well understood by assuming diffusive phonon scattering at grain boundaries, which limits the mean free path down to the grain size [78, 81, 82]. The electron transport should not be affected by the small grain size, since the electron mean free path in SiGe is already on the order of 1 nm. However, the power factor is actually affected by the nano sized grains; not many researchers have showed significant enhancement in ***ZT*** with small grains [83]. There have been some studies on electron transport in polycrystalline materials, not many of which can be applicable to nano sized grains. Among earlier studies, Fuchs and Sondheimer explored the average mean free path of electrons affected by the boundary of metal film structures [84]. More recently, Mayadas proposed a way to calculate the energy-dependent electron mean free path for grain boundary scattering by locating a scattering potential at grain boundaries using a delta function [85].

Along with the electron transport study in nanocomposites, porosity effects on transport properties are also explored. Experimental results in SiGe nanocomposites show that porosity in such nanocomposites can also degrade the electrical conductivity more significantly than the thermal conductivity so that a high figure of merit cannot be achieved [86]. In the 1970s, Lidorenko et al. reported up to a 30% increase in the ratio of the electrical conductivity to thermal conductivity for porous SiGe alloys and suggested a

possible enhancement in ***ZT*** using porous structures [87]. Recently, a possible enhancement in ***ZT*** by porous structures was suggested by several studies [88,89]. Song et al. presented experimental results on an anomalous reduction in the thermal conductivity of micro- and nano-sized porous films [88,89]. A modeling of two-dimensional nanocomposite structures has shown that the nanoscale porosity can cause significant reduction in the phonon thermal conductivity [90]. Nanoporous structures can also lead to an improvement in the Seebeck coefficient due to the energy filtering effect.

5.1 Bulk Modeling

In the diffusion regime, the charge and energy transport properties of bulk materials can be derived from solving the Boltzmann Transport Equation (BTE). Under the relaxation time approximation (RTA), an analytical solution of charge or phonon distribution functions can be expressed as a function of the mean free path or the relaxation time [91, 92]. Hence, the accuracy of this approach relies on how the relaxation time is determined. Functional forms of the relaxation time for various scattering mechanisms can be found in typical device physics textbooks and are listed in Table 5.1 [93]. In crystalline SiGe thermoelectric materials, the major scattering mechanisms for electrons are ionized impurity scattering and electron-acoustic phonon scattering. According to Mathiessen's Rule, the total scattering rate is obtained from taking the sum of the individual scattering rates, or the inverse of the relaxation times, when different scattering events happen

independently. The standard formulation based on the BTE, under the RTA, leads to the following expressions for the electrical conductivity and Seebeck coefficient [91]

$$\sigma = -\frac{1}{3}\int q^2\,\tau(E)v(E)^2\,\frac{\partial f(E_f,E)}{\partial E}\,\mathrm{D}\,(E)\mathrm{d}E \tag{5.1}$$

$$S = \frac{1}{3}\int q\,\frac{E-E_f}{T}\,\tau(E)v(E)^2\,\frac{\partial f(E_f,E)}{\partial E}\,\mathrm{D}\,(E)\mathrm{d}E\,/\,\sigma \tag{5.2}$$

where, E is the electron energy, E_F is the Fermi level, q is the electronic charge, τ is the momentum relaxation time, v is the group velocity of the charge carriers, f is the Fermi-Dirac distribution function, and D is the density of electronic states. This approach is similar to that of Vining [91], but more details are considered in this work. In particular, we calculate the Fermi level based on the measured carrier concentration, and we consider the non-parabolicity of the conduction band due to a high carrier concentration and the change in band structure with varying temperature and doping concentrations. The coefficients for the relaxation times associated with different scattering mechanisms are taken from the literature as described in Table 5.1.

Table 5.1 Electron Modeling Parameters

Majority carrier concentration	N (cm^{-3})
Effective mass of electrons of $Si_{1-x}Ge_x$ at X point[a]	$m_X=[1.08(1-x)+1.41x-0.183x(1-x)]m_e$ (kg)
Effective mass of electrons of $Si_{1-x}Ge_x$ at L point[a]	$m_L=[1.08(1-x)+0.71x-0.183x(1-x)]m_e$ (kg)
Effective mass of holes of $Si_{1-x}Ge_x$ at Γ point[a]	$m_\Gamma=(0.81-0.47x)m_e$ (kg)
Si energy gap at X point[a]	$Eg_{Si_X}=1.17-4.73\times10^{-4}T^2/(T+636)$ (eV)
Si energy gap at L point[a]	$Eg_{Si_L}=1.65-4.73\times10^{-4}T^2/(T+636)$ (eV)
Ge energy gap at L point[a]	$Eg_{Ge_L}=0.74-4.80\times10^{-4}T^2/(T+235)$ (eV)
Ge energy gap at X point[a]	$Eg_{Ge_X}=0.85Eg_{Ge_L}/0.66$ (eV)
$Si_{1-x}Ge_x$ energy gap at each point[a]	$Eg=Eg_{Si}(1-x)+Eg^*_{Ge}x-0.4x(1-x)-0.009\ln(N/10^{17})+\{[\ln(N/10^{17})]^2+0.5\}^{1/2}$ (eV)
Nonparabolicity[b]	$A=2$ (eV)
Electron density of states at X point[c]	$D_X=8\pi\sqrt{2E(1+(E/\alpha))}\sqrt{((m_X/h^2))^3}(1+(2E/\alpha))$
Electron density of states at L point[c]	$D_L=8\pi\sqrt{2E(1+(E/\alpha))}\sqrt{((m_L/h^2))^3}(1+(2E/\alpha))$
Hole density of states at Γ point[c]	$D_\Gamma=(8\pi\sqrt{2E(m_\Gamma)^3}/h^3)$
Dielectric constant of $Si_{1-x}Ge_x$ [a]	$\varepsilon=11.7+4.5x$
Screening length[d]	$L_D=\sqrt{4\pi\varepsilon\varepsilon_0kT/q^2N}$
Ionized impurity scattering rate[d]	$1/\tau_i=2\pi^2N/h(q^2L_D^2/4\pi\varepsilon\varepsilon_0)^2D_X$
Electron-phonon scattering potential[d]	$DA=-9.5$ (electron), 5.0 (holes) (eV)
Bulk moduli of $Si_{1-x}Ge_x$ [a]	$Cl=98-23x$ (GPa)
Electron-phonon scattering rate[d]	$(1/\tau_{e-p})=(2\pi^2kT/hcl)(D_X/6)DA^2$ (s^{-1})
Hole-phonon scattering rate[d]	$(1/\tau_{h-p})=(2\pi^2kT/hcl)D_\Gamma DA^2$ (s^{-1})
Lattice constant[a]	$a=0.002\,733x^2+0.019\,92x+0.5431$ (nm)
Alloy scattering potential[b]	$U_A=0.7$ (eV)
Alloy scattering rate (electrons)[e]	$(1/\tau_a)=x(1-x)(3a^3\pi^4U_A^2/32h)(D_X/6)$ (s^{-1})
Alloy scattering rate (holes)[e]	$(1/\tau_a)=x(1-x)(3a^3\pi^4U_A^2/32h)D_\Gamma$ (s^{-1})

Source: Hohyun Lee, Daryoosh Vashaee, D. Z. Wang, Mildred S. Dresselhaus, Z. F. Ren, and Gang Chen, Effects of nanoscale porosity on thermoelectric properties of SiGe, journal of applied physics 107, 094308, 2010.

Figure 5.1 shows the relaxation time for various scattering mechanisms vs. energy and temperature.

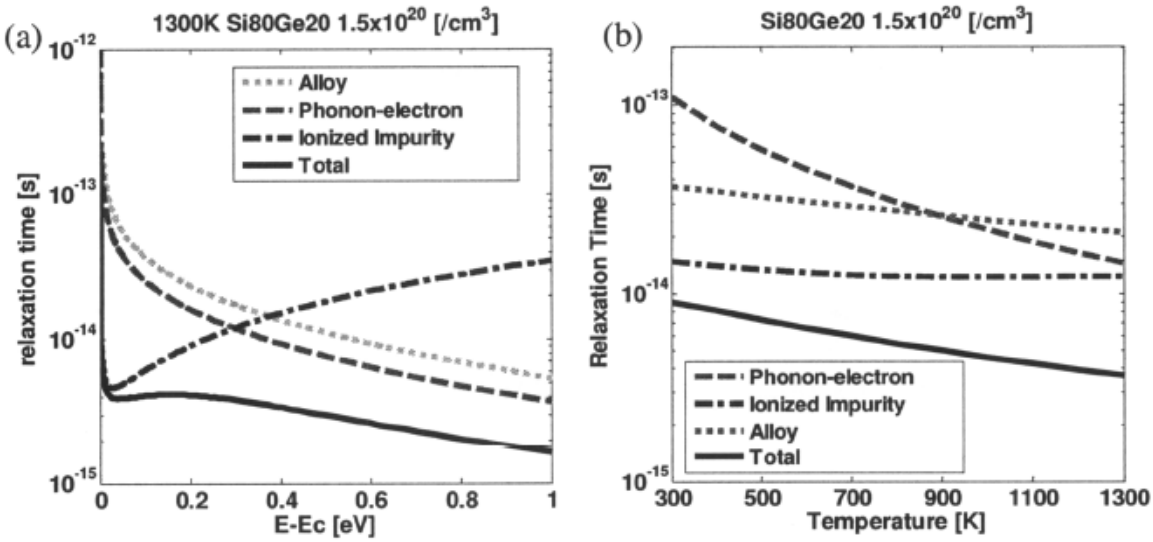

Figure 5.1 Relaxation time for different scattering mechanisms for: (a). different electron energies; (b). and for various temperature range.

Source: Hohyun Lee, Daryoosh Vashaee, D. Z. Wang, Mildred S. Dresselhaus, Z. F. Ren, and Gang Chen, Effects of nanoscale porosity on thermoelectric properties of SiGe, JOURNAL OF APPLIED PHYSICS 107, 094308, 2010.

The electron-phonon and alloy scattering rates are proportional to the square root of the electron energy. Both of the scattering mechanisms are related to lattice perturbations or imperfections, and the scattering rates are proportional to the number density of electrons (electron density of states), which is again proportional to the square root of electron energy (Table 5.1). Meanwhile, the ionized impurity scattering is induced by the Coulomb potential. The ionized impurity scattering is more effective for low energy electrons, since low energy electrons are more likely to be affected by a charge potential due to their low velocity (Fig.5.1 a). For a heavily doped sample, ionized impurity scattering is the most dominant scattering mechanism at all temperatures (Fig.5.1 b).

The expression for the electrical contribution to the thermal conductivity shares the same relaxation time as in the electrical conductivity or the Seebeck coefficient calculations. According to the Wiedemann-Franz law, the ratio of the electronic thermal conductivity to the electrical conductivity is proportional to temperature and the proportionality constant is called the "Lorentz number" [98]. In theory, the Lorentz number L is given by

$$L=\frac{\pi^2}{3}\left(\frac{k_B}{e}\right)^2 = 2.44 \times 10^{-8}\ [W\Omega K^{-2}] \tag{5.3}$$

where, k_B is the Boltzmann constant, and e is charge of an electron. The value of the Lorentz number is roughly constant, but not exactly the same for all materials and for all temperatures. Hence, the Lorentz number is calculated for different temperatures and different electrical conductivity ranges.

For modeling the lattice thermal conductivity, a similar approach is used. The simplified expression for the lattice thermal conductivity is

$$k=\frac{1}{3}\int C(\omega)\upsilon(\omega)\Lambda(\omega)d\omega \tag{5.4}$$

where, ω is the phonon frequency, C is the lattice heat capacity, υ is the sound velocity, and Λ is the phonon mean free path. Three-phonon scattering, point defect scattering, and phonon-electron scattering are considered in order to determine the phonon mean free path in the bulk SiGe alloy. The functional forms of each scattering rate and the required constants are listed in Table 5.2. The group velocity of acoustic phonons, i.e. sound velocity, divided by the total scattering rate is the mean free path. As in the case of electron modeling, mean free paths, calculated by various scattering

mechanisms, are superposed using Mathiessen's Rule. When the grain size is smaller than the bulk phonon mean free path, phonons will be scattered diffusively at grain boundaries. The grain is another source of scattering, and the effective phonon mean free path will be limited by the small grain size L [81].

$$\frac{1}{\Lambda_{effective}} = \frac{1}{\Lambda_{bulk}} + \frac{1}{L} \tag{5.5}$$

The actual functional forms for the lattice thermal conductivity are slightly more complicated than Equation (5.4) and are taken from studies in the 1960s (Table 5.2) [94].

Table 5.2 Phonon Modeling Parameters

Normalized phonon frequency	$\omega_N = h\omega / 2\pi k T_D$
Debye temperature of $Si_{1-x}Ge_x$ [a]	$T_D = 630 - 266x$ (K)
Atomic mass of $Si_{1-x}Ge_x$ [a]	$M = 28.09(1-x) + 72.61x$ (g/mol)
Cube root volume of $Si_{1-x}Ge_x$ [a]	$crv = \{[12.1(1-x) + 13.6x]/N_A\}^{1/3}$
Density of $Si_{1-x}Ge_x$ [a]	$\rho = 2329 + 3493x - 499x^2$ (kg/m^3)
Sound velocity[a]	$v = (2kT_D/h)(\pi/6)^{1/3}(crv/100)$ (m/s)
Anharmonicity parameter[b]	$\gamma = 0.91$
3 phonon Umklapp scattering rate[b]	$1/\tau_U = 3.264 \times 10^{-2} 19\gamma^2\omega_N^2 T/27\ Mcrv^2 T_D$ (s^{-1})
3 phonon Normal scattering rate[b]	$1/\tau_N = 2/\tau_U$ (s^{-1})
Point defect (alloy) scattering rate[b]	$1/\tau_{PD} = \{(28.09 - 72.61/M)^2 + 39[(12.1/N_A)^{1/3} - (13.6/N_A)^{1/3}/crv]^2\} \times 6.17 \times 10^{11} T_D \omega_N^4$ (s^{-1})
Phonon-electron scattering rate[b]	$1/\tau_{p-e} = 4DA^2 v(\pi m)^3/h^4 \rho(2kT/mv^2) \times \{\omega_N T_D/T - \ln 1 + \exp[(mv^2 - 2E_F)/2kT + \omega_N^2 T_D^2/8mv^2 kT^3 + \omega_N T_D/2T]/1 + \exp[(mv^2 - 2E_F)/2kT + \omega_N^2 T_D^2/8mv^2 kT^3 - \omega_N T_D/T]\}$ (s^{-1})
Boundary scattering rate[c]	$1/\tau_B = v/\text{grain}$
Combined scattering rate	$1/\tau_C = 1/\tau_U + 1/\tau_N + 1/\tau_{PD} + 1/\tau_{p-e} + 1/\tau_B$
I_1 [b]	$\int_0^1 \tau_C \omega_N^2((\omega_N T_D/T)^2 e^{\omega_N T_D/T}/(e^{\omega_N T_D/T} - 1)^2) d\omega_N$
I_2 [b]	$2\int_0^1 (\tau_C/\tau_U)\omega_N^2((\omega_N T_D/T)^2 e^{\omega_N T_D/T}/(e^{\omega_N T_D/T} - 1)^2) d\omega_N$
I_3 [b]	$2\int_0^1 (1/\tau_U)(1 - (2\tau_C/\tau_U))\omega_N^2((\omega_N T_D/T)^2 e^{\omega_N T_D/T}/(e^{\omega_N T_D/T} - 1)^2) d\omega_N$
Lattice thermal conductivity[b]	$4.67 \times 10^{-2}(I_1 + I_2^2/I_3) T_D^2/crv$

Source: Hohyun Lee, Daryoosh Vashaee, D. Z. Wang, Mildred S. Dresselhaus, Z. F. Ren, and Gang Chen, Effects of nanoscale porosity on thermoelectric properties of SiGe, JOURNAL OF APPLIED PHYSICS 107, 094308, 2010.

5.2 Charge Transport in Nanocomposites

When the bulk mean free path is much smaller than the grain size as in electrons, there should be no effect of grain size on the transport properties. However, a number of experimental studies suggest that electrical conductivities of nanocomposites are degraded with small grain sizes. This fact suggests that there exist scattering mechanisms for electrons other than the simple diffusive scattering of electrons at grain boundaries. There are two explanations for additional scattering sources at the grain boundaries. The first is a carrier trap at dangling bonds caused by defect sites along the grain boundaries [78]. When a grain is in contact with other grains, it is not likely to be aligned. A surface density of states will be created at misaligned grain boundaries and can trap electrons. Another explanation is that an excess amount of dopants are likely to form compounds with Si and precipitate at the boundaries in highly doped SiGe alloys [95]. Both can cause a potential difference at the boundaries, which behaves as a potential barrier for electrons. When a potential barrier exists, the electrical conductivity can be deteriorated more than the effect of simple diffusive scattering at the boundaries since electrons with low energy cannot go through the barrier easily. When the barrier height is low enough to be overcome by the thermal energy of electrons, we can also expect an energy filtering effect. Since the Seebeck coefficient is the measurement of the average energy of charge carriers, the Seebeck coefficient can increase by passing only high energy electrons over the energy barrier. Enhancement in the Seebeck coefficient is compensated by a decrease in the electrical conductivity so that the power factor may maintain or even increase for certain barrier heights [78].

The transmissivity calculations have been exploited in thin film structures. In thin films, the transmissivity of a film can be expressed as a function of the mean free path and the film thickness d by:

$$e^{\frac{\Lambda}{d}} = T \tag{5.6}$$

where, Λ is the mean free path caused by the boundary, and T is the transmissivity through a film. If we regard each grain in a nano composite as a film, then the grain size is equivalent to the film thickness d. The transmissivity in this equation is defined as how much energy is diminished for energy carriers with the mean free path Λ to travel a distance d.

For the multi-dimensional case, the transmissivity through composite structures can be calculated using the analogy between electromagnetic waves and electron waves. Electromagnetic wave propagation through particulate media or various structures has been widely studied throughout the last century [96]. The picture of a nanocomposite structure can be either particles in a host or an array of similarly-sized grains.

The transmissivity is defined as the portion of the incident diffusive radiation that reaches the other end of the unit cell. In both cases, we assume that the energy of the electrons is maintained but the direction is redistributed equally to any direction after transmission or reflection at the grain boundaries. The boundary scattering is considered to be independent of other scattering mechanisms so that the relaxation time by grain boundary scattering is combined with other scattering mechanisms using Mathiessen's rule. Also, the interactions between electrons are also neglected due to the short screening length compared to the distance between electrons [78].

Figure 5.2 shows the optimization of ***ZT*** for $Si_{80}Ge_{20}$ at 1300K. In addition to a grain size of 20nm, results for 5nm are also drawn in the same figure. 5nm is the size of an average particle before compaction. As the grain size gets smaller, the grain boundary density increases which results in strong grain boundary scattering.

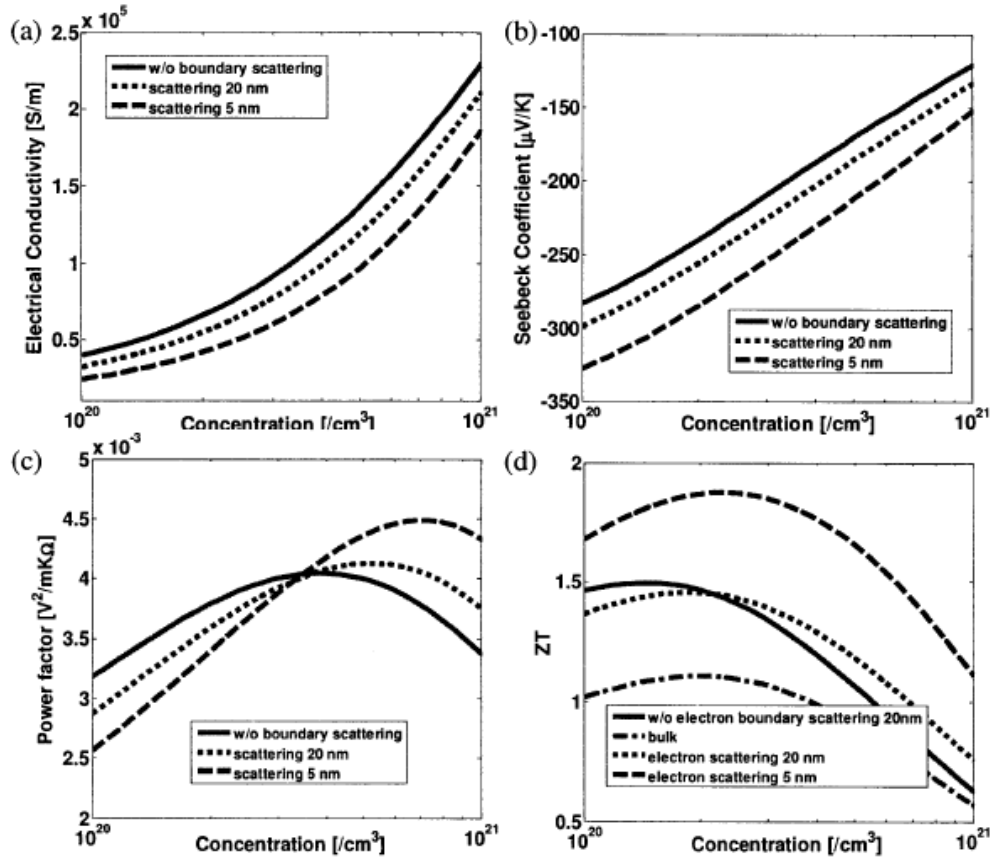

Figure 5.2 Optimization of ***ZT*** with respect to carrier concentration, considering electron grain boundary scattering. (a) Electrical Conductivity, (b) Seebeck Coefficient, (c) Power Factor, (d) ZT

Source: Hohyun Lee, Modeling and Characterization of Thermoelectric Properties of SiGe Nanocompostes, May 2009.

We could also observe the energy filtering effect by the scattering low energy electrons (Figure5.2 b). Although the power factor is less than the bulk values, at

concentration lower than $3.5x10^{20}/cm^3$, the power factor can be higher at high carrier concentrations (Figure 5.2 c). The actual measurement value can vary a little bit, because of the difference in potential height. Since the process still requires further optimization for batch fabrication, the morphology will be slightly different from sample to sample. Such differences in grain boundary shape will cause slight differences in the potential height and can cause ions. The maximum ***ZT*** happens at a lower concentration range as in the bulk case than the concentration for the maximum power factor, due to the high electronic thermal conductivity contribution (as can be inferred from the above figures). However, the optimal concentration for nanocomposites is slightly higher than that for bulk SiGe alloy, since the electronic thermal conductivity is slightly lower (Figure 5.2 d). The carrier concentration at 1300K, is between $3x10^{20}$ and $4x10^{20}/cm^3$. The corresponding ***ZT*** value is around 1.3 [78]. If we can control the carrier concentration at $2x10^{20}/cm^3$, we can expect further improvement in ***ZT*** up to 1.45. Moreover the ***ZT*** value does not change significantly at the concentration range between $1x10^{20}$ and $3x10^{20}/cm^3$ (Figure 5.2 d). Since it is difficult to control the carrier concentration at working temperature, the low sensitivity of ***ZT*** to carrier concentration is desirable for batch fabrication.

Since small grain size affects electron transport as well as the phonon thermal conductivity, there may exist an optimum grain size at which the maximum ***ZT*** is reached. Figure 5.3 shows the dependency of the power factor, lattice thermal conductivity, and ***ZT*** on grain size. Although the Seebeck coefficient increases slightly by grain boundary scattering, the power factor is reduced with smaller grain size due to severe degradation of the electrical conductivity. However, the grain size is more

effective in reducing the lattice thermal conductivity. Hence, smaller grain size leads to higher ***ZT***. Moreover, further enhancement in the power factor may be possible by the quantum confinement effect, when the grain size gets as small as half of the electron wavelength (~5 nm) [96].

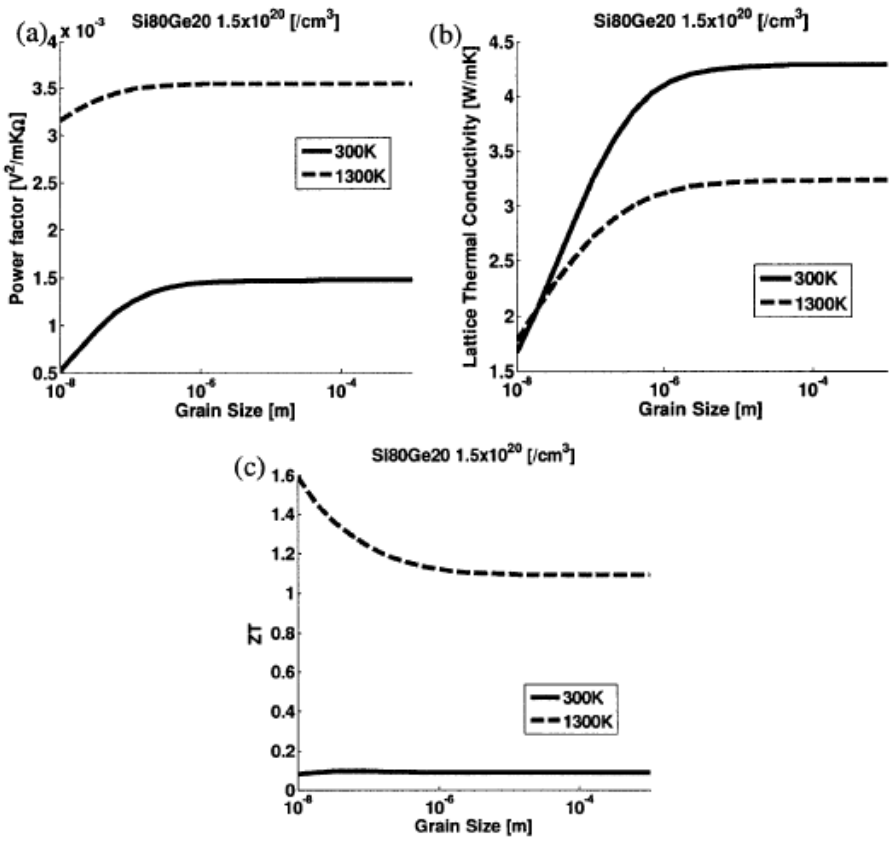

Figure 5.3 Optimization of ***ZT*** with respect to grain size. (a) Power Factor, (b) Lattice Thermal Conductivity, (c) ***ZT***.

Source: Hohyun Lee, Modeling and Characterization of Thermoelectric Properties of SiGe Nanocompostes, May 2009.

5.3 MATLAB

The name ‘Matlab’ comes from two words: matrix and laboratory. According to The MathWorks (producer of Matlab), Matlab is a technical computing language used mostly for high-performance numeric calculations and visualization. It integrates computing, programming, signal processing and graphics in easy to use environment, in which problems and solutions can be expressed with mathematical notation. Basic data element is an array, which allows for computing difficult mathematical formulas, which can be found mostly in linear algebra. But Matlab is not only about math problems. It can be widely used to analyze data, modeling, simulation and statistics. Matlab high-level programming language finds implementation in other fields of science such as biology, chemistry, economics, medicine and many more [97].

Most important feature of Matlab is easy extensibility. This environment allows creating new applications and becoming contributing author. It has evolved over many years and has become a tool for research, development and analysis. Matlab also features set of specific libraries, called toolboxes. Toolboxes are collecting ready to use functions that are used to solve particular areas of problems. Matlab System consists of five main parts. First, Desktop Tools and Development Environment are set of tools that are helpful while working with functions and files. Besides simple operations, more complex arithmetic can be calculated, including matrix inverses, Fourier transformations and approximation functions [97].

CHAPTER 6

RESULTS AND DISCUSSION

For the efficient thermoelectric energy conversion, both n-type and p-type materials should be developed. When one material has a low efficiency, the entire system efficiency will be limited by the low efficient material no matter how good the other material is. SiGe has been used for various space missions and conventional SiGe materials have ***ZT*** values of 0.9 and 0.5 at 1200K for n-type and p-type materials, respectively [98]. Using the nanocomposite approach, ***ZT*** values have been improved by up to a factor of two [99]. Moreover, by improving p-type SiGe materials up to efficiency that is similar to n-type materials, the device efficiency, using a nanocomposite pair, is highly improved compared to the conventional SiGe pair.

Ge is not as abundant as Si and is much more expensive, which increases the production cost of SiGe alloys. According to the modeling study in Chapter 5, an enhancement in ***ZT*** is still possible with a smaller amount of Ge. Using only 5% of Ge in n-type nanocomposite material, ***ZT*** is improved up to the level of $Si_{80}Ge_{20}$. In bulk materials, this enhancement cannot be possible due to the lower alloy scattering of phonons in low Ge ratio materials. However, the phonons scatter additionally at the large number of interfaces in nanocomposites, and, therefore, the thermal conductivity can be reduced to the alloy level, while maintaining a higher power factor due to the higher solubility limit and lower electron alloy scattering.

6.1 n-Type SiGe

The electronic contribution to the thermal conductivity (k_e) can be estimated, by models, using the Wiedemann-Franz law with the calculated Lorentz number.

For the reference, k_e = 0.77 W/m-K at room temperature with an electrical conductivity $\boldsymbol{\sigma}$=1.2 x 10^5 S/m, whereas for a typical nanostructured dense bulk sample, k_e = 0.55 W/m-K at room temperature for $\boldsymbol{\sigma}$ = 0.70x10^5 S/m. By subtracting the electronic contribution k_e from the total thermal conductivity k, the lattice thermal conductivity (k_L) of nanostructured samples is around 1.8 W/m-K at room temperature, which is about 47% of the lattice part k_L (around 3.8 W/m-K) of the reference material.

For the SiGe system, at T < 1000^0C, the lattice thermal conductivity is still the dominant heat transport mechanism. Therefore, it should be possible to further decrease the thermal conductivity by making even smaller grains [45].

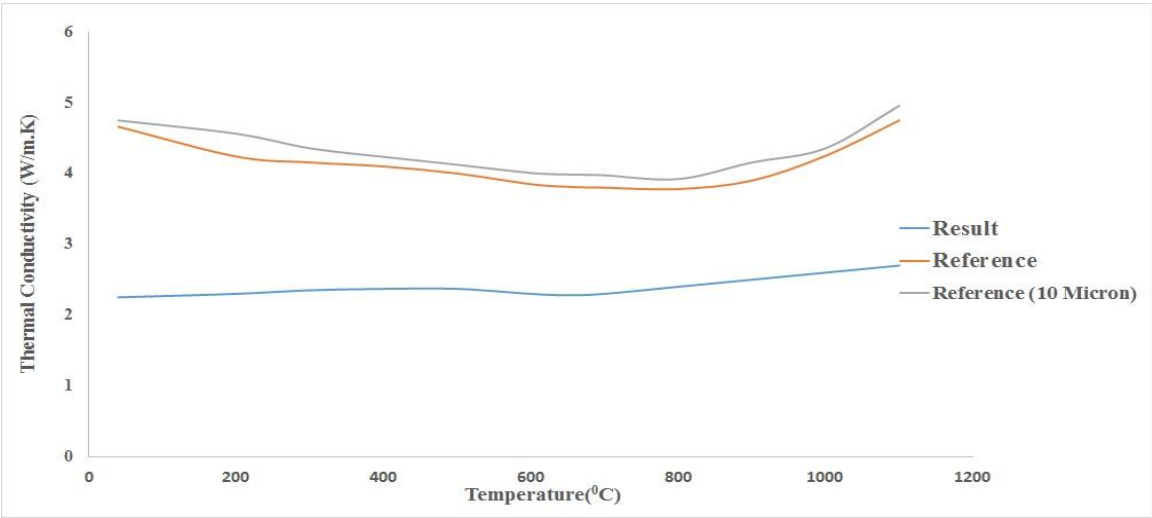

Figure 6.1 Thermal Conductivity VS Temperature Graph (n-Type $Si_{80}Ge_{20}$).

Reference: X.W.Wang and et al. Enhanced thermoelectric figure of merit in nanostructured n-type silicon germanium bulk alloy. *Appl. Phys. Lett.*, 93:193121, 2008.

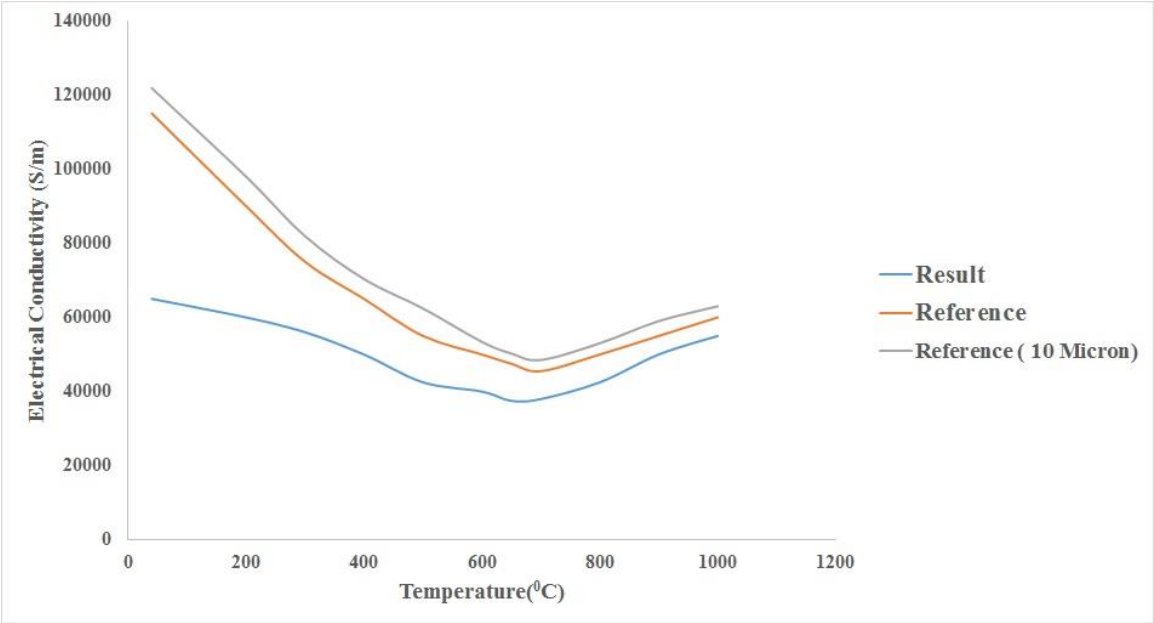

Figure 6.2 Electrical Conductivity VS Temperature Graph (n-Type $Si_{80}Ge_{20}$).

Reference: X.W.Wang and et al. Enhanced thermoelectric figure of merit in nanostructured n-type silicon germanium bulk alloy. *Appl. Phys. Lett.*, 93:193121, 2008.

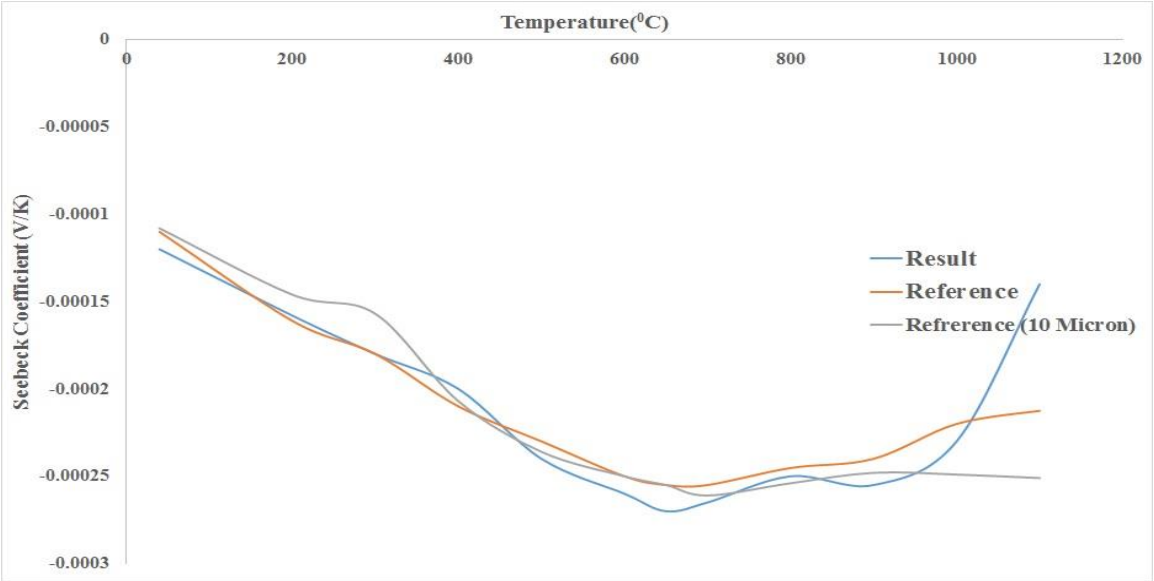

Figure 6.3 Seebeck Coefficient VS Temperature Graph (n-Type $Si_{80}Ge_{20}$).

Reference: X.W.Wang and et al. Enhanced thermoelectric figure of merit in nanostructured n-type silicon germanium bulk alloy. *Appl. Phys. Lett.*, 93:193121, 2008.

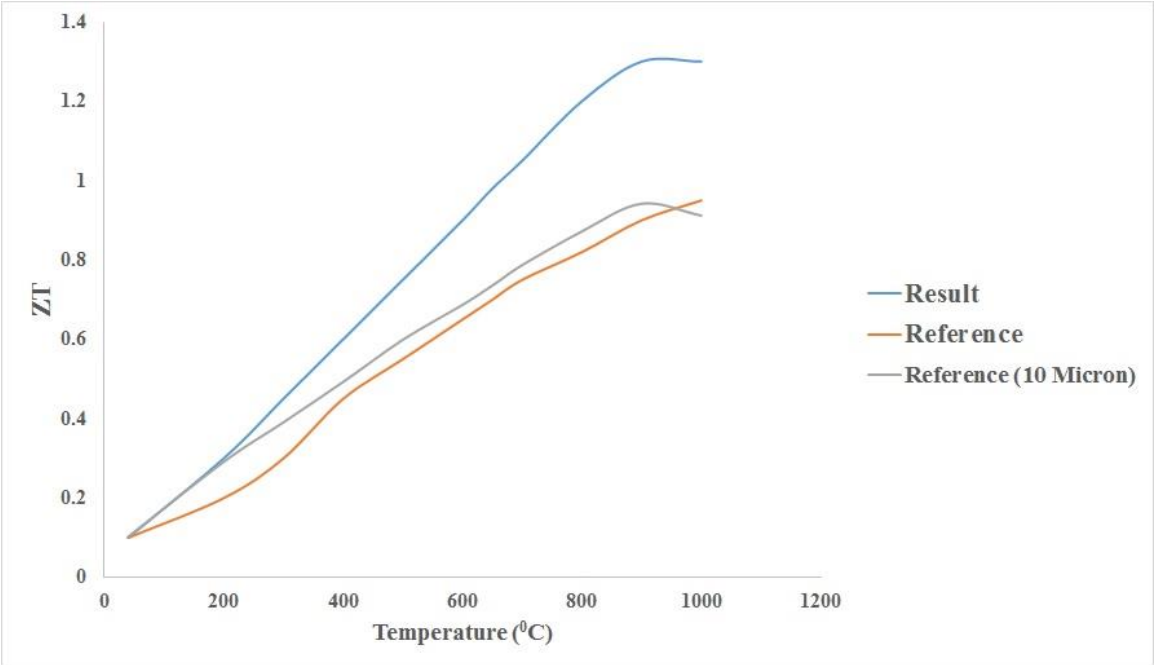

Figure 6.4 ***ZT*** VS Temperature Graph (n-Type $Si_{80}Ge_{20}$).

Reference: X.W.Wang and et al. Enhanced thermoelectric figure of merit in nanostructured n-type silicon germanium bulk alloy. *Appl. Phys. Lett.*, 93:193121, 2008.

The electrical conductivities of the nanocomposite samples are lower than that of the reference in the low temperature region, but similar above 750^0C. Lower electron mobility was measured in the nanostructured samples, leading to a lower electrical conductivity. The effect of potential barrier is less in the higher temperature range, since electrons are less affected by the potential barriers due to the higher thermal energy. While the potential barrier scatters low energy electrons, high energy electrons will go through the barrier without being disturbed. The energy filtering of low energy electrons leads to the enhancement in the Seebeck coefficient

For the nanostructured samples, the ***ZT*** value shows a maximum of about 1.3 at 900^0C, which is about 40% higher than the ***ZT*** (0.93) of the reference. The enhancement

is in the similar range as expected by the modeling study with the grain size of 20 nm (1.4 at 1300K). The significant improvement in ***ZT*** is mainly attributed to the thermal conductivity reduction. This reduction in the thermal conductivity is strongly correlated with the nanostructure features in our samples. In comparison, a previous study on n-type SiGe with grain size of 1 μm has a thermal conductivity about 72% of its bulk counterpart, but an electrical conductivity 68% of that of its bulk counterpart, leading to no improvement in ***ZT***. ***ZT*** improvements can be achieved by reducing the thermal conductivity more than the electrical conductivity. ***ZT*** can be enhanced further by optimizing the carrier concentration and reducing the grain size to 5 nm. The process conditions should be further explored to achieve these enhancements.

For device applications, the average ***ZT*** in the operating temperature range is the most valuable parameter rather than the maximum ***ZT***. The advantage of the newly developed nanocomposites is that the ***ZT*** value is maintained above 1.0 over a wide temperature range between 600 and 1000°C. This makes nano $Si_{80}Ge_{20}$ materials much more useful as high-performance thermoelectric materials for power generation with large temperature difference such as in solar radiation, radioisotope generated heat, and waste heat. The thermal stability of the nanostructured samples is a serious concern for thermoelectric materials since thermoelectric devices are required to operate at high temperatures for many years [45].

6.2 P-Type SiGe

As discussed in the previous section, dopant precipitation occurs between 800K and 1000K and hence the low temperature properties depend on the thermal history of the samples. More importantly, the thermal conductivity of the nanostructured bulk samples is much lower than that of the bulk micron grains sample over the whole temperature range up to 1000°C, which led to a peak ***ZT*** of about 0.95 in the nanostructured bulk samples of $Si_{80}Ge_{20}$. Such a peak ***ZT*** value is about 90% improvement over that of the p-type RTG SiGe alloy currently used in space missions, and 50% above that of the reported record value in the literature. The significant reduction in the thermal conductivity in nanostructured samples is mainly due to the increased phonon scattering at the numerous interfaces of the random nanostructures. Since the electronic thermal conductivity of the nanostructured bulk sample is similar to that of the RTG sample, the actual phonon thermal conductivity reduction is at least a factor of two based on the experimental data shown below in Figure 6.5.

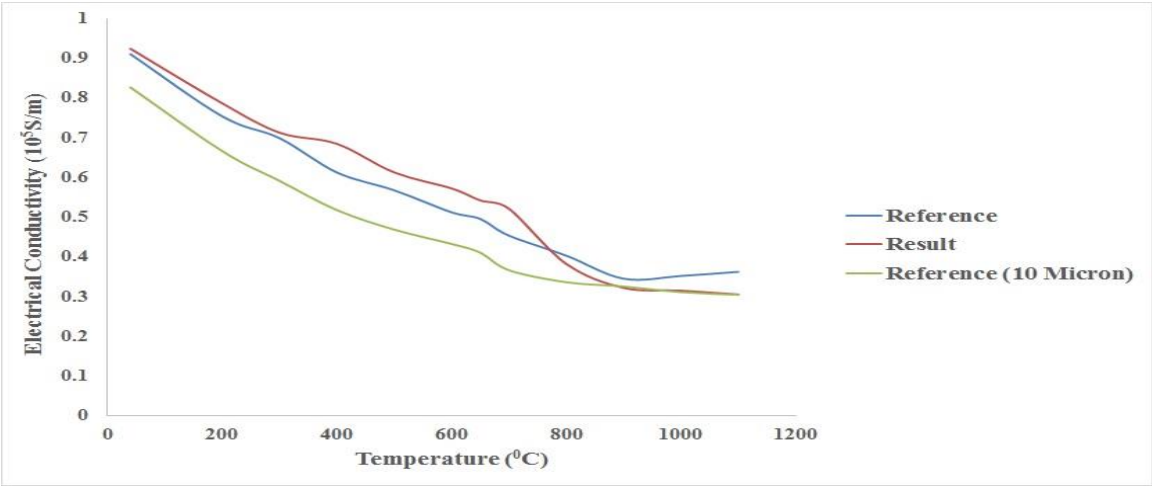

Figure 6.5 Electrical Conductivity VS Temperature Graph (p-Type $Si_{80}Ge_{20}$).

Reference: G. Joshi and et al. Enhanced thermoelectric figure-of-merit in nanostructured p-type silicon germanium bulk alloys. *Nano Letters*, 8(12):4670–4674, 2008.

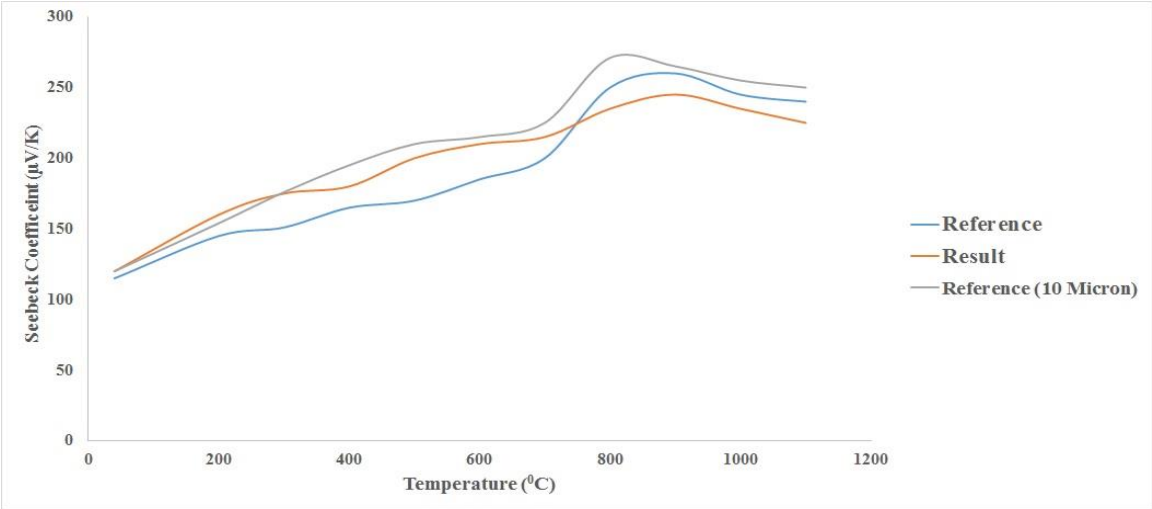

Figure 6.6 Seebeck Coefficient VS Temperature (p-Type $Si_{80}Ge_{20}$).

Reference: G. Joshi and et al. Enhanced thermoelectric figure-of-merit in nanostructured p-type silicon germanium bulk alloys. *Nano Letters*, 8(12):4670–4674, 2008.

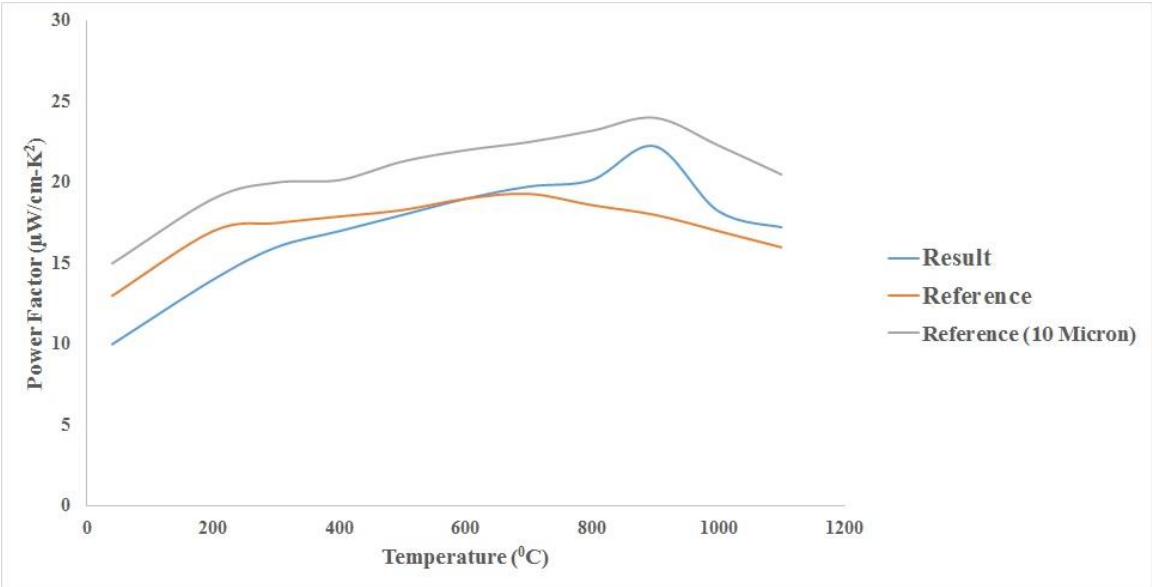

Figure 6.7 Power Factor VS Temperature (p-Type $Si_{80}Ge_{20}$).

Reference: G. Joshi and et al. Enhanced thermoelectric figure-of-merit in nanostructured p-type silicon germanium bulk alloys. *Nano Letters*, 8(12):4670–4674, 2008.

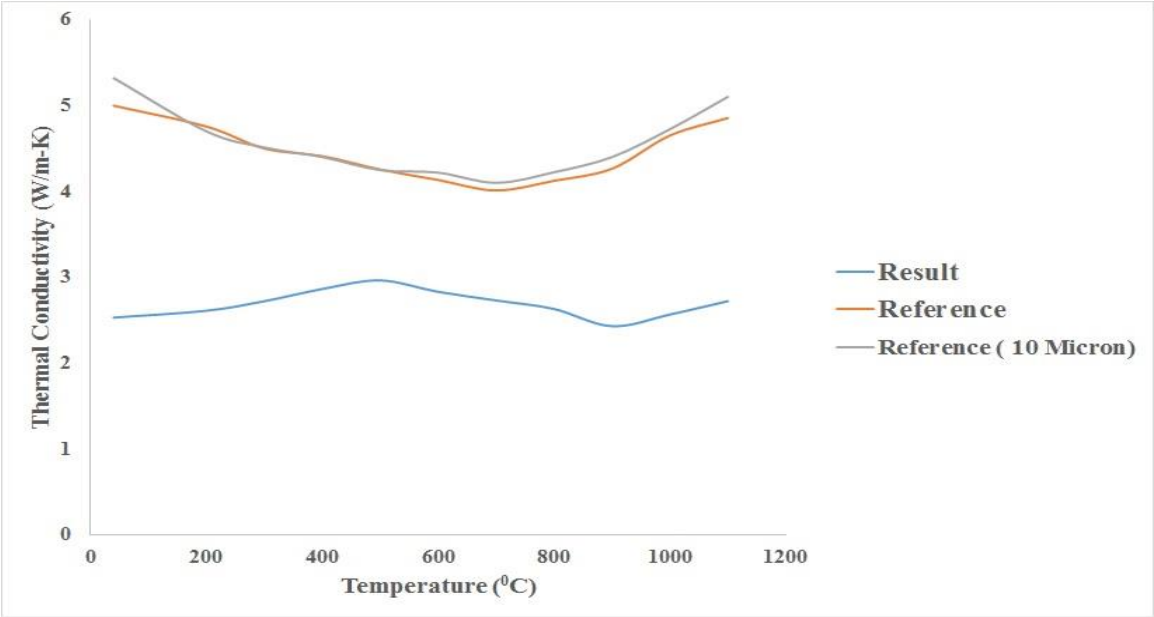

Figure 6.8 Thermal Conductivity VS Temperature (p-Type $Si_{80}Ge_{20}$).

Reference: G. Joshi and et al. Enhanced thermoelectric figure-of-merit in nanostructured p-type silicon germanium bulk alloys. *Nano Letters*, 8(12):4670–4674, 2008.

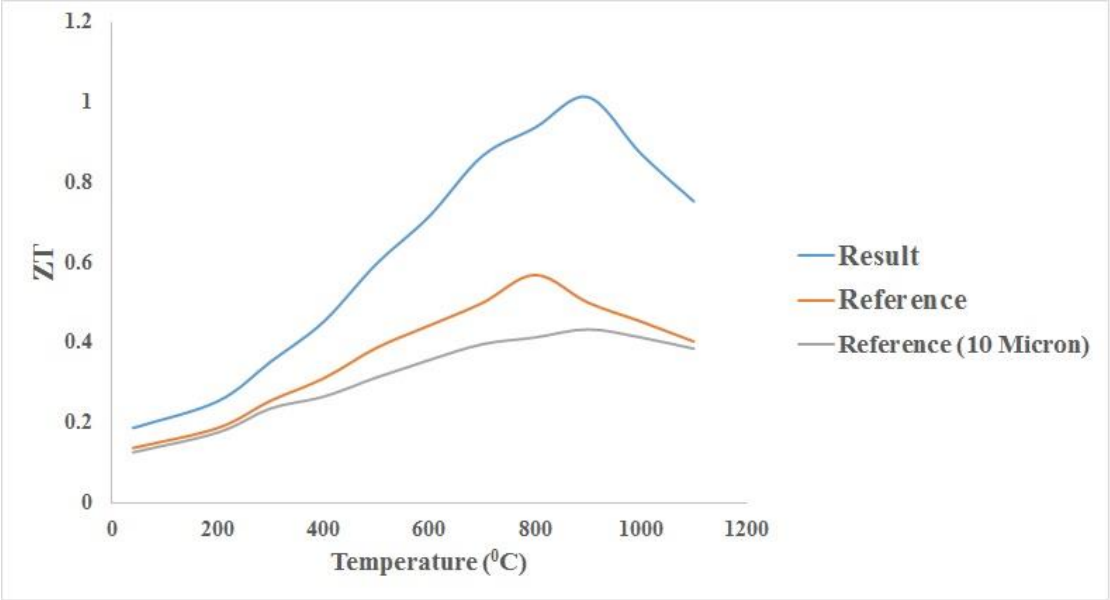

Figure 6.9 ***ZT*** VS Temperature (p-Type $Si_{80}Ge_{20}$).

Reference: G. Joshi and et al. Enhanced thermoelectric figure-of-merit in nanostructured p-type silicon germanium bulk alloys. *Nano Letters*, 8(12):4670–4674, 2008**.**

CHAPTER 7

CONCLUSIONS

A theoretical model for the thermoelectric properties of SiGe nanocomposite materials has been presented. In our theoretical model, we implemented different types of scattering mechanisms for both electrons and phonons scattering. We have seen that nano-structuring reduces the electrical conductivity of the materials. Electron transport in plycrystalline materials has had an important issue for electronic devices or photovoltaic cells as well as for thermoelectric materials. There have been explanations for the low electrical conductivity in multi-grained materials, but a good mathematical model has not been well-established. The modeling studies not only provide a good understanding of the transport phenomena, but also are helpful to develop good thermoelectric materials further.

We have observed a ***ZT*** enhancement for n-type and p-type SiGe alloys mostly due to the reduction in the thermal conductivity. Such a reduction came from both an alloying effect and increased phonon interface scattering. If the contribution of interface scattering dominates the reduction in the thermal conductivity, ***ZT*** can be enhanced without using a high Ge ratio. Reducing the amount of Ge also leads to a higher electrical conductivity due to a higher carrier concentration and less electron alloy scattering. So the power factor of the nano-structure materials also decreases with the thermal conductivity reduction. ***ZT*** is likely to be improved in nanograined SiGe.

Both p-type and n-type SiGe showed a ***ZT*** enhancement over conventional materials by up to a factor of two, and ***ZT*** was maintained over 1 over a wide range of

temperatures, which will be beneficial for high temperature power generation under large temperature differences. Such an improvement of thermoelectric materials will enhance the applications for thermoelectric devices, including in areas such as waste heat recovery, large scale solid-state refrigeration and power generations from renewable energy sources, and therefore will contribute to solving future energy – related and environmental problems. The enhancement in efficiency with nano-structures is still not large enough to compete with conventional power generation systems. However, in some circumstances, like off-grid remote area, the ability to generate power is more important than the efficiency of the system.

REFERENCES

1. Agency EE Energy and environment report 2008; 2008. (Accessed 01/21/2015).

2. Commission IE Efficient electrical energy transmission and distribution; 2007. (Accessed 03/02/2015).

3. J. R. Szczech, J. M. Higgins and S. Jin, Enhancement of the thermoelectric properties in nanoscale and nanostructured materials ,*J. Mater. Chem.*, 2011, 21, 4037-4055 DOI: 10.1039/C0JM02755C.

4. B. R. Nag. Theory of electrical transport in semiconductors. Pergamon Press, 1972.

5. G.S. Nolas, J. Sharp, and H. J. Goldsmid, Thermoelectrics: basic principles and new materials developments. Springer, 2001.

6. Th. J. Seebeck "Magnetische Polarisation der Metalle und Erze Durch Temperatur-Differenz"1822-23 in Ostwald's Klassiker der Exakten Wissenshaften Nr. 70 (1895). Seebeck Biography 1. Seebeck Biography 2.

7. L. Sebastien, P. Ghosez , First-principles study of the electronic and thermoelectric properties of $Ca_3Co_4O_9$, (2013).

8. C. Bera. Thermo electric properties of nanocomposite materials. Engineering Sciences, Ecole Centrale Paris, 2010. English. <NNT: 2010ECAP0027>.

9. G. A. Slack. CRC Handbook of Thermoelectrics. D. M. Rowe, 1995. (Accessed: 26/06/2015)

10. L. D. Hicks and M. S. Dresselhaus. Effect of quantum-well structures on the thermoelectric figure of merit. Physical Review B, 47:12727, 1993.

11. D. I. Bilc and P. Ghosez. Electronic and thermoelectric properties of Fe2VAl: The role of defects and disorder. Physical Review B, 83:205204, 2011.

12. Srinivasan Krishnamurthy, A. Sher, and A.-B. Chen. Band structures of SixGe1-x alloys. Physical Review B, 33(2):1026, January 1986.

13. L. Sebastien, P. Ghosez, First-principles study of the electronic and thermoelectric properties of $Ca_3Co_4O_9$, (2013).

14. Marisol Martín-González n, O. Caballero-Calero, P. Díaz-Chao, Nanoengineering thermoelectrics for 21st century: Energy harvesting and other trends in the field, www.elsevier.com/locate/rser , September 2012 (Accessed: 23/8/2015).

15. L. D. Hicks, T. C. Harman, and M. S. Dresselhaus. Use of quantum-well superlattices to obtain a high figure of merit from nonconventional thermoelectric materials. Applied Physics Letters, 63(23):3230, 1993.

16. D. G. Cahill, S. K. Watson, and R. O. Pohl. Lower limit to thermal conductivity of disordered crystals. Phys. Rev. B, 46:6131{40, 1992}.

17. The Mineral Sphalerite, http://www.minerals.net/mineral/sphalerite.aspx (Accessed; 02/10/2015).

18. Structure of Solids, Ionic Solids, The wurtzite Structure, http://minerva.mlib.cnr.it/mod/book/view.php?id=269&chapterid=106 (Accessed: 05/10/2015).

19. A. R. West, Basic Solid State Chemistry (1988), pp 238.

20. Rock Salt Structure, http://chemistrytextbookcrawl.blogspot.com/2012/08/rock-salt-structure.html. (Accessed: 09/06/2015).

21. N. W. Ashcroft and N. D. Mermin, Solid state physics, Holt, Rinehart and Winston, 1976.

22. Richard M. Martin. Electronic structure: basic theory and practical methods. Cambridge University Press, April 2004.

23. J. M. Ziman. Electrons and phonons. Clarendon Press, 2001.

24. D. Lacroix, K. Joulain, and D. Lemonnier, Monte carlo transient phonon transport in silicon and germanium at nanoscales. Physical Review B, 72(6), 2005.

25. C. Kittel and H. Kroemer. Thermal physics. W. H. Freeman, 1980.

26. C. M. Bhandari. CRC handbook of thermoelectrics, 1995.

27. G. S. Nolas, J. Sharp, and H. J. Goldsmid, Thermoelectrics: basic principles and new materials developments. Springer, 2001.

28. J. Singleton. *Band Theory and Electronic Properties of Solids*. Oxford University Press, 2001.

29. William Jones and Norman Henry March. Theoretical solid state physics. Wiley-Interscience, 1973.

30. J.M. Ziman. *Principles of the Theory of Solids*. Cambridge University Press, 1964.

31. T.S. Hutchison and D.C. Baird. *The Physics of Engineering Solids*. John Wiley and Sons, 1963.

32. Thompson, Daniel, "Thermoelectric Properties of Silicon Germanium: An In-depth Study to the Reduction of Lattice Thermal Conductivity" (2012). *All Dissertations.* Paper 984.

33. G.A. Slack, in: H. Ehrenreich, F. Seitz, D. turnbull (Eds.), Solid State physics, 34, Academic Press, 1979.

34. P. Pichanusakorn, P. Bandaru, Materials Science and Engineering R 67 (19) (2010) 19–63.

35. M. cutler, J.F. Leavy, R.L. Fitzpatrick, Physics Review 133 (1964) A1143–A1152.

36. D.M. RoweEd. Introduction, CRC Handbook of Thermoelectrics, 1995.

37. H. Alam, S. Ramakrishna, A review on the enhancement of figure of merit from bulk to nano-thermoelectric materials, Oct-2012.

38. M. S. Dresselhaus, G. Chen, M. Y Tang, G.Yang, H. Lee, D. Wang, Z. Ren, Jean- P. Fleurial, P. Gonga, New Directions for Low Dimensional Thermoelectric Materials-Advanced Materials (2007) 1043–1053.

39. E. R. Venkatasubramanian, T. Siivola, Colpitts, B. O Quinn, Nature 413 (11) (2001) 597–602.

40. R. Fletcher, M. Tsaousidou, P.T. Coleridge, Y. Feng, Z.R. Wasilewski, Physica E 12 (2002) 478–481.

41. Alexander Balandin, Kang L Wang, Journal of Applied Physics 84 (11) (1998) 6149–6153.

42. H.Bottner, G. Chen, R. Venkatasubramanian, MRS Bulletin 31 (2006).

43. R. Venkatasubramanian, Physics Review. B 61 (2000) 3091–3097.

44. C. Gould, N. Shammas, A Review of Thermoelectric MEMS Devices for Micro, Power Generation, Heating and Cooling Applications, Source: Micro Electronic and Mechanical Systems, Kenichi Takahata (Ed.), ISBN 978–953, 307–027, 2009.

45. M. Zebarjadi, K. Esfarjani, M.S. Dresselhaus, Z.F. Ren, G. Chen, Energy & Environmental Science 5 (2012) 5147–5162.

46. A.J. Minnich, M.S. Dresselhaus, Z.F. Ren, G. Chen, Energy & Environmental Science 2 (2009) 66–479.

47. Snyder. Thermoelectrics. http://www.its.caltech.edu/~jsnyder, (Dec 2014).

48. D.M. Rowe. *CRC Handbook on Thermoelectrics*. CRC Press, (1995).

49. M.C. Steele and F.D. Rosi. Thermal conductivity and thermoelectric power of germanium-silicon alloys. *J. App. Phys.*, 29:1517, (1958).

50. Thompson, Daniel, "Thermoelectric Properties of Silicon Germanium: An In-depth Study the Reduction of Lattice Thermal Conductivity" (2012).

51. Jean-Pierre Fleurial and et al. Improved n-type SiGe/gap thermoelectric materials. *Proceedings of the Eighth Symposium on Space Nuclear Power Systems*, page 451, 1991.

52. H. J. Goldsmid and A. W. Penn. Boundary scattering of phonons in solid solutions. *Phys. Lett. A*, 27:523, 1968.

53. J.E. Parrot. The thermal conductivity of sintered semiconductor alloys. *J. Phys. C.: Solid State Phys.*, 2:147, 1969.

54. D.M. Rowe and et al. Boundary scattering of phonons. *J. Phys. C: Solid State Phys.*, 11:1787, 1978.

55. D.M. Rowe and R.W. Bunce. The vacuum hot-pressing of germanium and silicon-germanium Alloys. *J. Phys. D: Appl. Phys.*, 10, 1977.

56. R.A. Lefever, G.L. McVay, and R.J. Baughman. Preparation of hot-pressed silicon-germanium ingots: Part i-iii. *Materials Research Bulletin*, 9(7):685–692, 735–744, 863–872, 1974.

57. C. Vining. A model for the high temperature transport properties of heavily doped n-type Silicon Germanium alloys. *J. Appl. Phys.*, 69:331, 1991.

58. J.W. Vandersande, C. Wood, and S. Draper. Improved gap doped size thermoelectric material. *Mater. Res. Soc. Symp. Proc. 97*, 97:347, 1987.

59. B.A. Cook and et al. The preparation of si-ge thermoelectric materials by mechanical alloying. *Proceedings of Intersociety Energy Conversion Engineering Conference*, 2:693, 1989.

60. B. A. Cook, J. L. Harringa, S. H. Han, and B. J. Beaudry. Parasitic effects of oxygen on the thermoelectric properties of si80ge20 doped with gap and p. *Journal of Applied Physics*, 72(4):1423–1428, 1992.

61. B.A. Cook and et al. Oxygen effects in mechanically alloyed si80ge20 doped with gap and p. *Mater. Res. Soc. Proc.*, 234:111, 1991.

62. B.A. Cook and et al. Thermoelectric properties of mechanically alloyed p-type si80ge20 alloys. *Proceedings of the Eighth Symposium on Space Nuclear Power Systems*, page 431, 1991.

63. B.A. Cook and et al. Optimization of the p/ga ratio in n-type si80ge20 thermoelectric alloys prepared by mechanical alloying. *Proceedings of the 11th International Conference on Thermoelectric Energy Conversion*, page 28, 1992.

64. A. Balandin and et al. Electron and phonon energy spectra. *Phys. Rev. B*, 66:245319, 2002.

65. A. Balandin and et al. Mechanism for thermoelectric. *Appl. Phys. Lett.*, 82:3, 2003.

66. M. Lee and Venkatasubramanian. Effect of nanodot. *Appl. Phys. Lett.*, 92:053112, 2008.

67. V. Siklitsky. Silicon germanium. http://www.ioffe.rssi.ru, May 2012.

68. L. Vegard. Die konstitution der mischkristalle und die raumfllung der atome. *Zeitschrift fr Physik*, 5:17, 1921.

69. J.P. Dismukes, L. Ekstrom, and R.J. Paff. Lattice parameter and density in germanium-silicon alloys. *J. Phys. Chem.k*, 68(10):3021–3027, 1964.

70. C. B. Vining, W. Laskow, J. O. Hanson, R. R. Van der Beck, and P. D. Gorsuch. Thermoelectric properties of pressure-sintered si0.8ge0.2 thermoelectric alloys. *Journal of Applied Physics*, 69(8):4333–4340, 1991.

71. X.W.Wang and et al. Enhanced thermoelectric figure of merit in nanostructured n-type silicon germanium bulk alloy. *Appl. Phys. Lett.*, 93:193121, 2008.

72. G. Joshi and et al. Enhanced thermoelectric figure-of-merit in nanostructured p-type silicon germanium bulk alloys. *Nano Letters*, 8(12):4670–4674, 2008.

73. G.H. Zhu and et al. Increased phonon scattering by nanograins and point defects in nanostructured silicon with a low concentration of germanium. *PRL*, 102:196803, 2009.

74. Chandan. Bera and et al. Thermoelectric properties of nanostructured si1-xgex and potential for further improvement. *J. Appl. Phys.*, 108:124306, 2010.

75. Sabah K. Bux and et al. Nanostructured bulk silicon as an effective thermoelectric material. *Adv. Funct. Mater.* 19:24452452, 2009.

76. Robert Crowe. Industry leaders: Sun shot's $1 per watt goal feasible. http://www.renewableenergyworld.com, May 2012. (Accessed: 08/23/2015).

77. Bo Yu and et al. Enhancement of thermoelectric properties by modulation-doping in Silicon Germanium alloy nanocomposites. *Nano Lett.*, 12:2077–2082, 2012.

78. G. Chen, in Recent Trends in Thermoelectric Materials Research III; Vol. 71 (2001), p. 203-259.

79. J. P. Heremans, C. M. Thrush, and D. T. Morelli, Journal of Applied Physics 98, 063703 (2005).

80. X. B. Zhao, X. H. Ji, Y. H. Zhang, T. J. Zhu, J. P. Tu, and X. B. Zhang, Applied Physics Letters 86, 062111 (2005).

81. A. Minnich and G. Chen, Applied Physics Letters 91, 073105 (2007).

82. R. G. Yang, G. Chen, and M. S. Dresselhaus, Nano Letters 5, 1111-1115 (2005).

83. G. A. Slack and M. A. Hussain, Journal of Applied Physics 70, 2694 (1991).

84. E. H. Sondheimer, Advances in Physics 1, 1 (1952).

85. A. F. Mayadas and M. Shatzkes, Physical Review B 1, 1382 (1970).

86. H. Lee, D. Z. Wang, M. Y. Tang, Z. F. Ren, P. Gogna, J.-P. Fleurial, M. S. Dresselhaus, and G. Chen, in International Conference on Thermoelectrics (Clemson, SC, 2005).

87. N. S. Lidorenko, O. M. Narva, L. D. Dudkin, and R. S. Erofeev, Inorganic Materials 6, 1853 (1970).

88. D. Song and G. Chen, Applied Physics Letters 84, 687-689 (2004).

89. D. W. Song, W. N. Shen, B. Dunn, C. D. Moore, M. S. Goorsky, T. Radetic, R. Gronsky, and G. Chen, Applied Physics Letters 84, 1883-1885 (2004).

90. R. G. Yang, G. Chen, and M. S. Dresselhaus, Nano Letters 5, 1111-1115 (2005).

91. C. B. Vining, Journal Of Applied Physics 69, 331 (1991).

92. G. Chen, Nanoscale Energy Transport and Conversion: A Parallel Treatment of Electrons, Molecules, Phonons, and Photons (Oxford University Press, 2005).

93. M. Lundstrom, Fundamentals of Carrier Transport, Second Edition ed. (Cambridge, 2000).

94. N. W. Ashcroft and N. D. Mermin, Solid State Physics, 1st ed. (Brooks Cole, 1976).

95. B. A. Cook, J. L. Harringa, S. H. Han, and C. B. Vining, Journal Of Applied Physics 78, 5474 (1995).

96. L. D. Hicks and M. S. Dresselhaus, Physical Review B 47, 12727 (1993).

97. J. Inglot, Advanced Image Processing with Matlab, May 2012.

98. H. Lee, Modeling and Characterization of Thermoelectric Properties of SiGe Nanocompostes, May 2009.

99. A. Samarelli, L.Ferre, Llin, Prospects for SiGe thermoelectric generators, www.elsevier.com/locate/sse, April 2014.